Quasi-Periodicity and Dynamical Systems: An Experimentalist's View

JAMES A. GLAZIER AND ALBERT LIBCHABER

Abstract—**A great variety of natural and artificial systems exhibit chaos and frequency locking associated with quasi-periodicity. In this tutorial paper we present an overview of current theoretical and experimental work on quasi-periodicity. In Section I, we discuss the concept of universality and its relevance to experiments on nonlinear multifrequency systems. In Section II, we describe the reduction of experimental data by means of Poincaré sections, and the mathematical properties of the one-dimensional circle map. In Section III, we present the various dynamical systems techniques for determining scaling and multifractal properties as well as other more traditional methods of analysis. We emphasize the experimental observations that would support or refute the one-dimensional circle map model. In Section IV, we summarize the experimental results, concentrating on forced Rayleigh–Bénard convection and solid state systems. In Section V, we conclude with a brief discussion of the accomplishments and open problems of the dynamical systems theory of quasi-periodicity.**

I. Introduction

THE phenomenon known today as *frequency locking* was discovered over three hundred years ago when the Dutch physicist Christian Huygens noted that the pendula of two clocks placed near each other tended to synchronize [74]. This effect, in which an oscillator adjusts its frequency in response to a periodic stimulus (either externally or internally generated), is used today in many electronic systems requiring precise control of frequencies. Examples including the phase locking circuitry of atomic clocks, in which a quartz oscillator is locked to a Cesium standard, radio receivers, stereo turntables, and disk drives.

In the natural world, systems which exhibit frequency locking behavior are almost bewildering common; the most visible example being the moon, whose orbital and rotational periods are locked in a one-to-one ratio because of dissipative tidal forces. In any system in which two or more frequencies couple nonlinearly, either because of external perturbations or internal generation, a rich variety of effects can occur, including frequency locking, quasi-periodicity, pattern formation, intermittency, period doubling and other subharmonic generation, and both temporal and spatial chaos. It is sobering even to attempt to list the systems which have been examined experimentally: in mechanics, the damped driven pendulum [3], [34], [60], [101]; in hydrodynamics, the vortices behind an obstacle in a wind tunnel or an airplane wing [122], the dripping of a faucet [116], the convective rolls in a heated pan of water, and the oscillations of acoustically driven helium [82], [121]; in chemistry, the Belousov–Zhabotinsky reaction, the Chlorite–Thiosulphate reaction and many others [38], [111]; in solid state physics, charge density waves in niobium selenide [22], and other compounds [117], the conductivity of barium sodium niobate [94], oscillations in Josephson junctions [105], and in germanium [62], [72], in biology, cardiac cells [45], the brain [10], the slime mode *dictyostelium discoideum* [104], menstrual cycles in human females, and elsewhere [136]. This list could probably be extended almost indefinitely. We refer the reader interested in additional reading on experiments and theory to the bibliographies contained in the many surveys of specialized topics [11], [15], [33], [49], [102], [108], [128], [137].

One major characteristic of the above list is that, though all of its members exhibit complicated multifrequency behavior, they seem to share almost no other features. It is clearly impossible to produce a single theory which describes the detailed behavior of all of them. A theory which describes voltage oscillations in Josephson junctions can scarcely be expected to describe the life cycle of slime molds. A further problem is that full mathematical descriptions are not known for many of these systems; often, when the equations are known, they are effectively insoluble.

For a long time these various effects were seen as unrelated, if occasionally useful, curiosities. It required the development of a new branch of physics to allow us to appreciate them for what they are, the diverse results of a single elegant and simple theory. We find that if we examine all these systems at a high enough level, that is if we ignore detailed causes, they can be grouped into a few classes of generic behavior. This concept of *universality*—that seemingly unrelated systems can behave in essentially the same way—is central to many recent advances in physics. A Fortran programmer knows instinctively the lesson that physicists have had to learn with effort: it is the result of the program, not the particular machine language implementation that matters. In this case the "high level language" is, *dynamical systems theory*, the formalism which describes complicated behavior and chaos in terms of sequences produced by the repeated iteration of simple functions, and the relation of these iterated functions to the "machine code" of differential equations.

We may illustrate this point by considering an example from our own research [95]. The behavior of a fluid in a

Manuscript received September 25, 1987.
The authors are with The James Franck and Enrico Fermi Institutes, The University of Chicago, Chicago, IL 60637.
IEEE Log Number 88201084.

0098-4094/88/0700-0790$01.00 ©1988 IEEE

box, heated from below (Rayleigh–Bénard convection) has been studied for almost a hundred years [83]. Yet, 10 years ago, if you had asked a theoretical physicst to predict the flow pattern in such a box of fluid subject simultaneously to a magnetic field, heating and an alternating injected current, he would probably have said that it would be complicated and, because the result would apply only to one specialized system, uninteresting. If you had convinced him to try to calculate the flow he would have written down three coupled nonlinear partial differential equations (the Navier Stokes equation for the fluid flow and transport equations for the current and heat) and paused, for, with realistic boundary conditions, the equations would be completely intractable. To proceed further he would have assumed simplified boundary conditions, linearized the equations about a known solution [26], and with luck (for even the linearized equations are non-trivial to solve), produced an "approximate solution."

This answer would have had two fundamental problems: 1) changing the boundary conditions or the geometry even slightly would require resolving the whole problem from scratch; and 2) the answer would be both quantitatively and qualitatively wrong, because the linearization would be invalid in the range of parameters of interest. In particular, in the region of chaotic behavior, the "approximation solution" would be completely meaningless.

Today, despite extraordinary advances in computers and the techniques for solving partial differential equations, a physicist could still not solve the problem asked above. Except in the most trivial cases the Navier–Stokes equations remain insoluble. However, as first shown by Lorenz in his classic work on convection and weather prediction [87], in certain types of Rayleigh–Bénard convection we can predict many properties with excellent numerical accuracy without solving any differential equations at all. Indeed, for the small aspect ratio, forced Rayleigh–Bénard system, many of the calculations described in this article could be done with nothing more elaborate than a programmable calculator. Furthermore, the results we obtain for the Rayleigh–Bénard system apply, with only minor modifications, to many of the other systems we listed above. Using the techniques of dynamical systems theory, we can attain a universal result without a detailed solution to the underlying equations of motion.

We should add a note of caution. The dynamical systems approach is not a panacea. There are classes of questions, just as there are classes of systems, and we will discuss in this paper the sorts of questions our "high level" theory can answer. One thing we can definitely not predict is the detailed motion of a large volume of fluid in space and time. Though originally developed in the context of Hamiltonian systems, the iterated map approach discussed in this paper works best in heavily damped (or dissipative) systems in which most of the degrees of freedom are suppressed and only a few contribute to the behavior. In fact, the existing theory is only well developed for systems with one or two independent degrees of freedom. Fortunately, most of the systems on our list have this property. However, if we want to design an airplane wing, or a turbine, both of which depend on true many dimensional effects, we still need to solve the Navier–Stokes equations in detail. For the same reason we cannot address the problem of turbulence using existing dynamical systems techniques. With these caveats in mind we may turn to the theory of systems with two degrees of freedom.

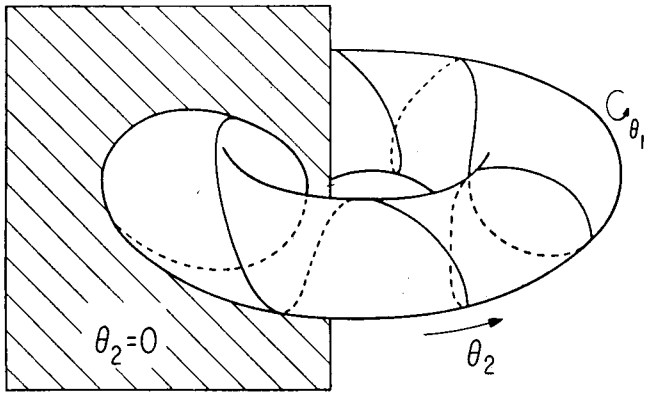

Fig. 1. Schematic diagram of a two frequency torus and a Poincaré section. The helical line on the torus traces out the system's trajectory in phase space. Angular coordinates θ_1 and θ_2 are indicated. The vertical plane indicates the stroboscopy at times $i\tau$. The Poincaré section is the intersection between the plane and the system trajectory. From [76].

II. Theory of the Circle Map

From Phase Space to the Iterated Map

Let us consider the simplest possible two-frequency system, two uncoupled harmonic oscillators with frequencies f_1 and f_2. We may characterize the state of the system by coordinates describing the amplitude of the oscillators x_1 and x_2 and their time derivatives $\dot{x}_1$ and $\dot{x}_2$. In this simple case, we can immediately reduce the number of variables to two by expressing both coordinate pairs in terms of angular coordinates $\theta_1 \equiv f_1 t$ and $\theta_2 \equiv f_2 t$, with $x_1 = \sin(\theta_1)$, $\dot{x}_1 = f_1 \cos(\theta_1)$, etc. $\cdots$. We can understand this system in a simple geometrical way. If we make a rotation by 360° correspond to $\theta = 1$ and identify $\theta \cong \theta + 1$, we may represent the time evolution of the system as a helical motion on a torus with the small diameter corresponding to θ_1 and the large diameter corresponding to θ_2, as shown in Fig. 1. Even this trivial system exhibits two qualitatively distinct behaviors depending on the ratio f_1/f_2, the number of rotations in the θ_1 direction per rotation in the θ_2 direction. If $f_1/f_2 = p/q$ is rational, then the motion is periodic, and the path will close after q circuits around the big circle. We say that the system is *periodic with period q* and completes *p cycles per period*. If, on the other hand, f_1/f_2 is irrational, then the path never intersects itself and the trajectory will cover the torus densely, that is, the trajectory will come arbitrarily close to any point on the torus. A system containing two or more incommensurate frequencies is said to be *quasi-periodic*.

Visualizing a torus is inconvenient. We can simplify the picture by using the equivalent of a strobe light to freeze the motion in the θ_2 direction and to eliminate the frequency f_2 from the problem. If we record θ_1 at a fixed

time interval $\tau \equiv 1/f_2$ and define $\theta_i \equiv \theta_1(i\tau)$, we flash the strobe at the frequency f_2, and take a slice through the torus at a fixed value of θ_2 as indicated by the vertical plane shown in Fig. 1. It is a general theorem [36] that the structure of the stroboscopy we obtain will be the same for almost all (in a measure theoretic sense) choices of θ_2. We have now reduced our four-dimensional problem to one dimension. We may therefore encode all of the dynamics of the problem in the form of a map from the circle onto itself, where the *return map*, $F(\theta)$ is defined by $\theta_{i+1} = F(\theta_i)$. In our example of a uniform rotation, $F(\theta)$ is the rotation map, $F(\theta) = \theta + \Omega$, where $\Omega = f_1/f_2$. For an arbitrary system we will obtain a return map of form, $F(\theta) = \theta + \Omega + f(\theta)$, f_1 will vary with f_2, and the period of the sequence $\{\theta_i\}$ will not equal the denominator of Ω. In this case it is convenient to describe the frequency of the system using the *winding number* [17], [76]:

$$W \equiv \lim_{i \to \infty} \frac{\theta_i - \theta_0}{i}$$

which is, in fact, the measured frequency ratio, f_1/f_2. In the case of uniform rotation, $W = \Omega$. If W is rational $\{\theta_i\}$ will be a finite periodic set of points, if irrational, $\{\theta_i\}$ will be quasi-periodic and cover the circle densely.

This formalism may seem elaborate for the problem in hand, but it does yield one immediately useful result. We have reduced a problem on the torus to the study of a map from the circle to itself.

In a real experiment, we measure the value of an oscillating variable T, at times $i\tau$ as described above, and plot T_i versus T_{i+1}. This produces a tangled one-dimensional loop or a finite set of discrete points lying on a bumpy and folded surface, not a smooth circular doughnut. A theory of Takens [112], [131] assures that this attractor contains the same information as a plot of T versus $\dot{T}$. For many purposes, e.g., the calculation of a local scaling or of a fractal dimension, this folded attractor is perfectly adequate. However, if we wish to calculate a return map, or an $f(\alpha)$ spectrum (to be discussed later) we must map the two-dimensional pairs (T_i, T_{i+1}) into the θ_i's, using a method developed by Thomae [77], [124] in which we measure the unknown winding number by plotting the time series versus a known rotation frequency (or the stroboscopy T_i versus iW) and looking for a one-dimensional Lissajous pattern.

We pick a W and plot T versus Wt. If we have chosen W correctly, the periods of the experimental data and W will correspond and we will obtain a one-dimensional curve as seen in Fig. 11 column 1. If our guess is close but not exact, we will see a gradually drifting Lissajous pattern. We repeatedly guess values of W and plot the results until we obtain a satisfactory agreement. An experienced operator with good data can calculate W to one part in 10^5 in four or five iterations. Using this W we can define an unambiguous order on the experimental attractor and assign a value of θ to each point. It is then a simple matter to calculate the return map or the $f(\alpha)$ spectrum. Unfortunately this method only works efficiently for one-dimensional sets and hence cannot be used in the strongly chaotic regime where many experiments show fundamentally two-dimensional behavior.

At this point it is helpful to introduce a few definitions. The reduction of a continuous time series to a discrete sequence $(\{T_i\})$ using stroboscopy is known as *taking a Poincaré section* [28], [37] and may be employed in an arbitrary number of dimensions. The plot of T_i versus T_{i+1} (versus $T_{i+2}, \cdots$ in higher dimensions) is the *Poincaré section*. It is also called an *attractor* because all points initially lying in some volume containing it, rapidly iterate towards it. This attraction is equivalent to the damping of an initial transient or perturbation. A given system may have more than one attractor for the same parameters, in which case it is said to be *multistable*. The reduction of the attractor to the $\{\theta_i\}$ form is known as *unwinding* and the resulting sequence $\{\theta_i\}$ is called an *orbit*. Because of the fundamental equivalence of these two representations, we shall use the terms orbit, section and attractor, interchangeably.

In an arbitrary two variable system the reduction procedure can break down at any point. It may not be possible to eliminate the time derivatives. If it is, the set of points produced by taking the Poincaré section may be a two-dimensional cloud, not a loop or finite set of points (this is the case for many strongly chaotic systems). It is the surprising experimental fact that many systems do produce one-dimensional Poincaré sections that makes the one dimensional theory discussed below useful.

The Circle Map

We next consider a slightly more complicated return map, which we will use as our model for the rest of this paper. We define the one-dimensional *standard circle map*, or *sine map* by

$$F(\theta) = \theta + \Omega - \frac{k}{2\pi} \sin(2\pi\theta).$$

In an experimental system, we define Ω to be the ratio f_1^0/f_2, where f_1^0 is the natural unperturbed oscillation frequency. The exact choice of the function $\sin(2\pi\theta)$ is not critical in this definition. Essentially any function with a single cubic inflection point will yield identical qualitative and similar quantitative behavior. The relative independence of the properties of the iterates on the exact form of the map makes the sine map model very general.

The big advance from the rotation map discussed in the previous section, is that we now have a nonlinear term with an adjustable strength and hence can examine what happens as we vary the nonlinearity. For $k = 0$ we are back to the linear situation described above, but for $0 < k \leqslant 1$ the situation is more interesting. $F(\theta)$ is still a simple invertible map of the circle onto itself, but the winding number W, no longer equals Ω. Each irrational W corresponds to a unique Ω as before. However, there is a finite interval $[\Omega_{W,1}, \Omega_{W,2}]$ over which the iterated map achieves each rational $W = p/q$ and $\{\theta_i\}$ (we should really write $\{\theta_i(k, \Omega)\}$) is periodic with period q. We say that the

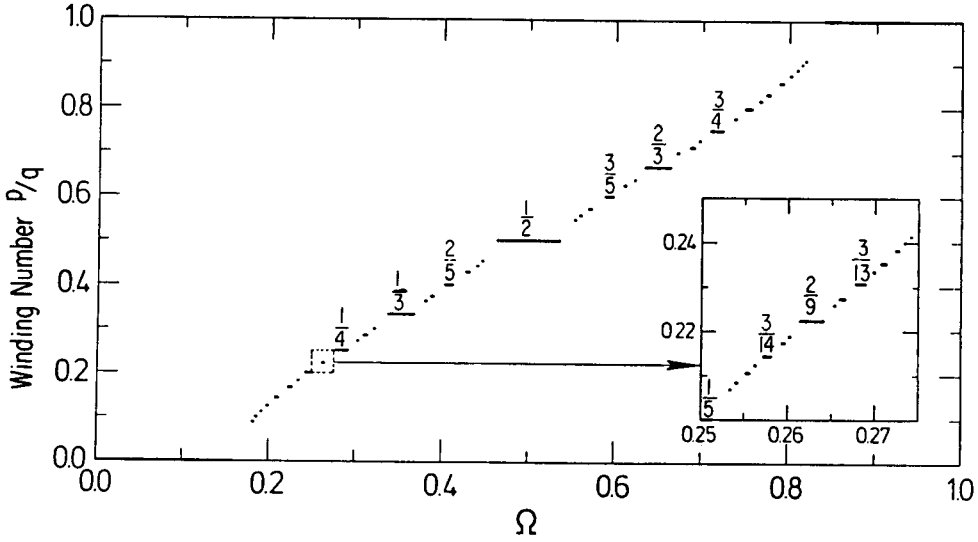

Fig. 2. Devil's staircase for the critical circle map. The steps indicate the regions in which W is constant. Fractions indicate W for a few of the wider steps. Inset shows an expanded view of the indicated section of the staircase. The structure of the sub-region is the same as that of the entire curve. From [76].

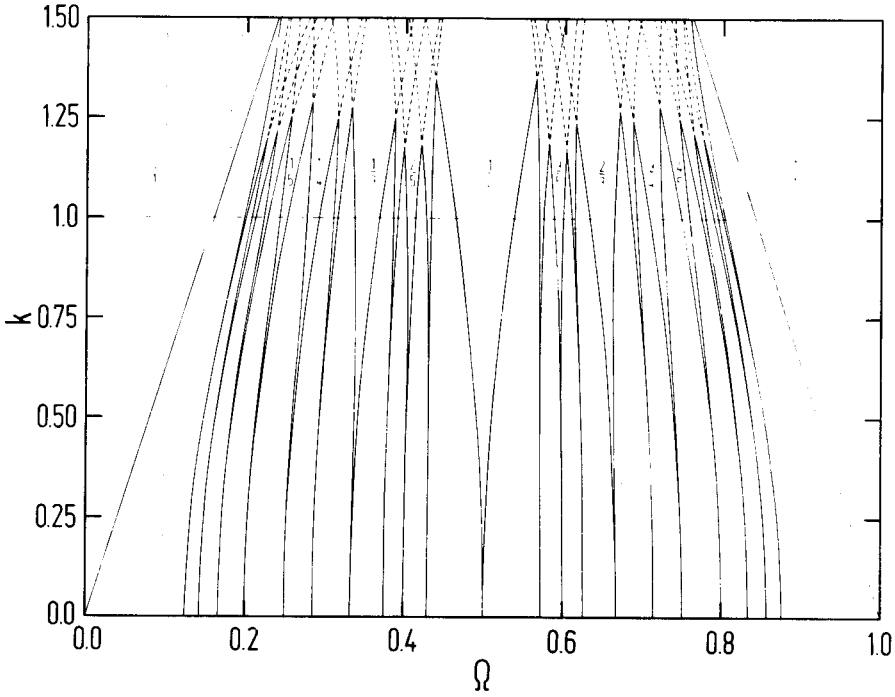

Fig. 3. Arnol'd tongue diagram. The pattern of locked tongues is shown in the Ω versus k plane for the first few Farey orders. The fractions indicate the winding number achieved inside the tongues. The relative widths of the tongues decrease as the tongue denominator increases and the tongues bend away from each other. The tongues do not overlap below the $k=1$ critical line. From [76].

equation *locks* to the winding number W over the interval. Experimentally, when the frequency f_2 is changed, there is a transient during which f_1 gradually "pulls in" to the appropriate ratio to f_2. The function $W(\Omega)$ forms a *Devil's Staircase* [12], a monotonic increasing continuous function, with plateaus of finite width at every rational W. We show the Devil's staircase for the sine map at $k=1$ in Fig. 2. The plateaus are *self-similar*; that is, if we enlarge any given segment of the staircase, its texture remains the same, as shown in the inset of Fig. 2.

As we increase the strength of the nonlinearity k, the width of each locked interval increases. If we plot these regions in the k versus Ω plane they form a series of slightly distorted narrow triangles (known as *Arnol'd Tongues* [7]) with their apices on the $k=0$ axis as shown in Fig. 3. Each tongue represents a region in parameter space associated with a particular rational winding number and we will refer to the tongue associated with a winding number p/q as the *p/q-tongue*. Surprisingly, for $k \leqslant 1$ the tongues bend away from each other and do not overlap.

The area covered by the locked regions increases smoothly and monotonically from 0 at $k=0$ to 1 at $k=1$. At $k=1$ (the *critical line*) almost any Ω yields a rational W and the set of Ω corresponding to irrationals forms a fractal of measure 0. Above the critical line ($k>1$), $F(\theta)$ is no longer invertible. The tongues begin to overlap, leading to hysteresis effects and chaos. Inside the tongues there are period doubling cascades leading gradually to chaotic motion (the "period doubling" route to chaos). Outside the tongues the remaining quasi-periodic orbits disappear abruptly, giving rise to further chaotic orbits (the "quasi-periodic" route to chaos).

The non-overlapping of tongues below $k=1$ implies that the width of a tongue corresponding to a rational winding number with denominator q,$(w(q))$ must decrease rapidly as q increases. We may make a quick estimate as follows: The number of tongues with a denominator q, $n(q)$ is of order q (strictly $n(q) \underset{q\to\infty}{\to} n$). The total width is $w \sim \sum_{q=1}^{\infty} q \cdot w(q)$. For w to remain finite requires $w(q) \sim q^{\beta}$ where $\beta < -2$. Detailed calculations by Bohr, Bak, and Jensen yield the result that at $k=1$, $\beta = -2.29$ [17].

Irrational Numbers

Because the circle map distinguishes strongly between rational and irrational winding numbers, it is worth recalling a few facts about irrationals and methods of approximating them by sequences of rationals. Approximating an irrational by truncating its finite decimal expansion is universally familiar. We will discuss a different method here. Any irrational number, $\sigma \in [0,1]$ can be uniquely represented in *continued fraction* form [7], [28] as

$$\sigma = \cfrac{1}{n_1 + \cfrac{1}{n_2 + \cfrac{1}{n_3 + \cdots}}}$$

where the n_i are positive integers. This formula may be written more conveniently as $\sigma \equiv \langle n_1, n_2, n_3, \cdots \rangle$. If we truncate the expansion after i terms we may define $\sigma_i \equiv \langle n_1, \cdots, n_i \rangle = p_i/q_i$. This yields a sequence of rational approximants, known as the *truncation sequence*, converging to σ: $\{\sigma_i\} \underset{i\to\infty}{\to} \sigma$.

The truncation sequence is closely related to the Farey ordering of the rationals [2]. For any pair of rational numbers $p/q < p'/q'$ we define their *Farey sum*

$$\frac{p''}{q''} = \frac{p}{q} \oplus \frac{p'}{q'} \equiv \frac{p+p'}{q+q'}.$$

This sum has three properties: 1) $p/q < p''/q'' < p'/q'$, 2) p''/q'' is the rational with smallest denominator between p/q and p'/q', and 3) if $|pq' - p'q| = 1$ then p''/q'' is in lowest terms. If we construct a "Farey tree" by starting with 0 and 1 and Farey adding nearest neighbors at a given level, property 3) will always be satisfied. We can then construct an approximation sequence converging to σ by successively bracketing σ and taking appropriate Farey sums. We define $\sigma_0' = 0$ and $\sigma_1' = 1$ and let $\sigma_i' = \sigma_{i-1}' \oplus \sigma_j'$ where j is chosen as large as possible such that σ_j' lies on the opposite side of σ from σ_{i-1}'. The sequence $\{\sigma_i'\}$ is in some sense the "best" approximation to the given irrational. It is the sequence of fractions with lowest monotonically increasing denominators which converge to σ. These lowest denominator tongues are the widest so the "best" sequence is the most significant to the experimentalist. In general the sequence $\{\sigma_i\}$ will be a subset of $\{\sigma_i'\}$ as the reader may easily verify by examining the sequence of fractions in Figs. 2 and 3.

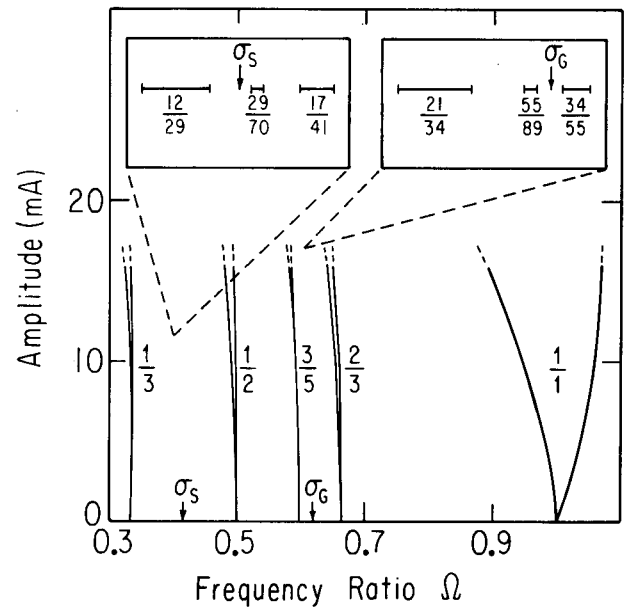

Fig. 4. Experimental Arnol'd tongue diagram for small aspect ratio forced Rayleigh–Bénard convection in mercury. The tongues are shown in the Ω versus A plane. The numbers indicate the winding number achieved inside the tongue. Insets show the relative widths of tongues near the golden (σ_G) and silver (σ_S) means and mark the position of the critical line. The widths and spacings of these tongues may be used to calculate the fractal dimension and scaling of the unlocked critical set. From [123].

These notions allow us to characterize the "degree of irrationality" of an irrational. We say that a number is strongly irrational if it is hard to approximate by rationals. In particular, numbers which have continued fractions of form $\langle n_1, n_2, \cdots, 1, 1, 1, \cdots \rangle$ are the most strongly irrational. The *golden mean*, $\sigma_G \equiv (\sqrt{5}-1)/2 = \langle 1,1,1,\cdots \rangle$ is the simplest of these. Of all irrationals in the interval [0,1], it is furthest from rationals of any given denominator. The golden mean has several other convenient properties. The sequence given by truncation of the continued fraction is the "best" sequence, and the terms are easily calculable: $\sigma_{i+1} = \sigma_i \oplus \sigma_{i-1} = F_i/F_{i+1}$ where F_i is the ith Fibonacci number defined by $F_{i+1} = F_i + F_{i-1}$ for $i \geq 1$, $F_0 = 0$ and $F_1 = 1$. Because of its distance from rational approximants, the golden winding number is the easiest place to observe quasi-periodicity experimentally (other winding numbers are more likely to lock to low denominator tongues). Thus the majority of both experimental and theoretical work on quasi-periodicity has been done at the golden mean. A second, slightly less irrational, winding number often selected for study is the silver mean, $\sigma_S \equiv \sqrt{2}-1 = \langle 2,2,2,\cdots \rangle$, for which $\sigma_{i+1} = \sigma_i \oplus \sigma_i \oplus \sigma_{i-1}$. The positions

of σ_G and σ_S and a few of their approximants are indicated in Fig. 4.

We must be a bit careful when we consider the notation for periodic states. For rational winding numbers $f_1/f_2 = p/q$ the notation means that the system returns to its original state after p cycles in f_1 or q cycles in f_2. Thus we cannot in general divide out common factors between p and q (the use of the Farey construction guarantees that common factors will not appear accidentally). A period doubling represents the appearance of low frequency subharmonics at $f_1/2$ and $f_2/2$. The time the period doubled system takes to return to its original state is now twice as long, but the ratio f_1/f_2 is the same. We denote this state using the somewhat bizarre looking notation $2 \otimes p/q$ or $2p/2q$. It may help to think of p and q as elements in a matrix, rather than as a fraction. We denote a state with multiplicity m by writing it out in terms of its prime factors, e.g., a period-18 state would be denoted $3^2 \otimes 2 \otimes p/q$ and call it a *period m* or *multiplicity m* state. There are also additional conventions for distinguishing the qualitative nature of such highly multiplied states which need not concern us here.

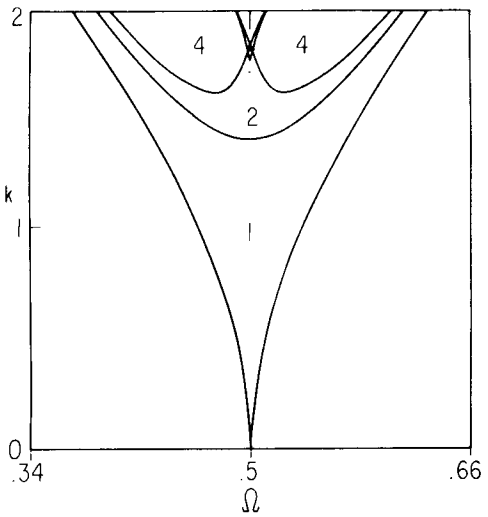

Fig. 5. Subharmonic structure of an Arnol'd tongue. A theoretical calculation of the period doubling structure of the 1/2-tongue for the circle map is shown in the Ω versus k plane. The lines in the tongue indicate the borders between different periodic states. The areas labelled by n correspond to $n \otimes 1/2$ states. Overlaps indicate regions of multistability. Note the symmetry breaking at periods 4 and the sequence of doubling. From [114].

III. Experimentally Verifiable Predictions

With this basic mathematical formalism we can consider the ways in which an experimental system might behave like a circle map. We will pay particular attention to the feasibility of measurements and to experimental behaviors which are imcompatible with the circle map model.

Global Structure

We have already discussed the typical pattern of Arnol'd tongues produced by the circle map. The presence of a heirarchy of locked states with a unique locked tongue for each rational winding numbers is the most characteristic feature of this map. Other systems which exhibit frequency locking, like phase locked loops, will typically lock only one fixed frequency ratio [34]. Because we do not expect the experimental system to correspond exactly to the simple circle map, we can not hope for exact quantitative correspondence in all aspects of the tongue structure. Nevertheless, the ordering of the tongues and their relative widths as given by the Farey construction are robust, as is the presence of a well-defined critical line. No missing or duplicated tongues are possible. Below the critical line, tongues do not overlap. There is no hysteresis (each value of k and Ω yields a unique winding number) and only periodic and quasi-periodic states exist. Above the critical line tongues overlap with hysteretic and multistable effects and only periodic and chaotic states exist. For higher dimensional iterated maps there is, in general, no single well-defined critical line and tongues can split and merge in complicated patterns [8], [90].

The sequence of states leading from periodic to chaotic motion within a tongue has been studied by MacKay and Tresser [90], Schell, Fraser, and Kapral [114], and by Glass and Perez [13], [45], [58], [107]. They find that above criticality, the locked states in the tongue undergo Feigenbaum period doubling [28], [43]. That is, the length of time (number of iterations) the system takes to return to its initial condition successively doubles. This corresponds to a splitting of the torus into 2^n overlapping sheets, where n is the order of the doubling. In the Poincaré section, each point of the locked state splits into 2^n distinct points. The separation between successive doublings decreases in accord with the Feigenbaum theory [33], and at a critical value of $k = k_c$, the *accumulation point of the cascade*, the period becomes infinite, i.e., the state becomes chaotic. For still higher k the full bestiary of complicated multiplicities predicted by Metropolis, Stein, and Stein is expected [28], [97], [99], however, the overlapping of tongues makes it difficult to observe experimentally [18]. We present the first few doublings for the 1/2-tongue as calculated by Schell, Fraser, and Kapral, in Fig. 5. The first doubling is symmetric and occurs in a single U-shaped band across the tongue. Higher doublings are composed of at least two distinct doubled states centered in the right- and left-hand sides of the tongue. The orbits of these states are different and "break the symmetry" of the tongue. The order in which these periods appear is generic to all one-dimensional circle maps with cubic inflection points. The presence of a different sequence in experimental observations would rule out identification with the circle map [27].

Scaling

We have noted that we do not expect quantitative correspondence between experimental and theoretical tongue widths. However, the sensitivity of tongue widths to the exact form of the circle map decreases for large denominators. At smaller length scales the locking sees only the narrow region around the inflection point of $F(\theta)$, much as a Taylor series sees only its lowest order terms for small arguments, so we expect that the ratios of

tongue widths or tongue separations for large denominators will be universal quantities depending only on the order of the inflection point. There are many such ratios or *scalings* which can be calculated. We have already mentioned one in passing, the ratio between the k intervals for period doubling bifurcations. However, we will discuss the Shenker δ [32], [118] (corresponding to the Feigenbaum δ for the logistic map [43]) which is the most easily calculated from experimental data. Choose an irrational σ and let w_i be the width of the tongue corresponding to the winding number σ_i in the truncation series. We then define

$$\delta_\sigma \equiv \lim_{i\to\infty} \frac{w_{i-1}-w_i}{w_i - w_{i+1}}$$

or equivalently,

$$\delta_\sigma \equiv \lim_{i\to\infty} \frac{w_i}{w_{i+1}}.$$

Depending on the system, either the first or the second definition may converge more rapidly. It may be helpful to refer to Fig. 4 to see that this limit makes sense around σ_G and σ_S. Renormalization group analysis by Shenker, Shraiman, Bohr, and others gives $\delta_{\sigma_G} = 2.833$ and $\delta_{\sigma_S} = 6.799$ [32], [76], [118]. Fortunately for the experimentalist, the limit converges rapidly and it is only necessary to measure tongues with denominators up to ≈ 100 to obtain a value of δ to a few percent.

Fractal Dimension

We have mentioned that at $k=1$ the set of Ω corresponding to irrational winding numbers is a fractal of measure 0. Fractals are objects whose apparent density or length changes depending on the length scale examined [92]. Such objects are ubiquitous in nature, classic examples being coastlines (which are short if measured in mile lengths but inconceivably long if measured at the scale of a grain of sand), the pattern of branches in a tree, the silhouette of a mountain, and cloud formations [113]. In mathematics the best known example (and a close analogue to the set under consideration) is the Cantor set consisting of all the numbers between 0 and 1 which have no 1's in their ternary expansion.

All objects are characterized by a dimension (δ) which describes how their volume (V) changes with length scale (l). For an ordinary object: $V \sim l^\delta$, where δ is an integer. The dimension of a fractal is determined in exactly the same way except that, in the case of a set of points we use not volumes but an effective number of points. We may define the *fractal dimension*, D, by the method known as box counting [53], [54], which resembles measuring an area by counting squares on a piece of graph paper. Consider a volume containing the set to be measured and divide it into rectangular n-dimensional boxes of side l. Let $N(l)$ be the number of boxes containing one or more points. Then, in the limit $l \to 0$, $N(l) \sim l^{-D}$. For a normal object, the two methods yield identical integer results. For a fractal the dimension can be any positive real number. The only restrictions on this method are that the embedding dimension, n, must be larger than $D+1$ and the minimum sample of the points goes like 10^D. The latter means that box counting is an inefficient way to calculate dimensions, and there exist myriads of specialized tricks for calculating the dimensions of particular systems [56].

As an example we describe the calculation of the dimension of the set of irrational winding numbers at $k=1$, first by box-counting and then using a trick. Let $w(l)$ be the total width of locked tongues on the interval [0,1] which have width greater than or equal to l. Then $1-w(l)$ is the total width of the regions which are unlocked at this length scale (i.e., for which the denominator of the winding number is too large). Therefore the number of unlocked boxes at this length scale is $N(l) = (1-w(l))/l$. We then calculate the fractal dimension D by the box counting method, as $D = -\lim_{l\to 0}(\log(N(l))/\log(l))$. Numerical computations by Jensen, Bak, and Bohr [76] give $D = 0.87 \pm 3.7\times 10^{-4}$.

For the experimentalist, measuring an arbitrarily large number of tongues to determine $w(l)$ is impractical. It is much more convenient to use a local method developed by Hentschel and Procaccia [73], which depends only on the scaling of the spacing between three Farey neighbors and yields a result within a few percent of the fractal dimension. If we pick an irrational σ and look at the "best" sequence of rational approximants we can obtain a fair approximation to D as follows: let S_i be the length of the interval between the tongues corresponding to σ'_{i-1} and σ'_i. Let S'_i and S''_i be the lengths of the intervals between these two tongues and the tongue corresponding to σ'_{i+1}. See Fig. 4. Then we may define D' by

$$\lim_{i\to\infty} \left\{ \left(\frac{S'_i}{S_i}\right)^{D'} + \left(\frac{S''_i}{S_i}\right)^{D'} \right\} = 1.$$

The numerically computed value of D' for the circle map is $D' = 0.868 \pm 0.002$. Again, as in the computation of scaling constants, one need only measure tongues with denominators up to about 100 to obtain experimental values of D' to a few percent. Like D, D' is the same for a wide variety of maps similar to the sine map. This method has the additional advantage that it establishes an implicit relationship between local dimension and scaling.

The Multifractal Spectrum

The frequency locking structure at the critical line is not the only fractal generated by the circle map. For irrational winding numbers, the Poincaré section itself is fractal at the critical line. The local density or scaling (α) is nonuniform as seen in Fig. 12. That is, if we measure the density of the Poincaré section at different points we obtain different results. The simple fractal dimension is less useful for such sets, since it averages out much of the structure. We would like to be able to characterize inhomogeneities in scaling consistently. There are two different ways to view the problem, leading to equivalent results.

The first is the method of *generalized dimensions*, D_q defined by Hentschel and Procaccia [73]. We examine the moments of the density distribution, much as we would the

multipole expansion of an electric field, and repeat the basic fractal dimension calculation keeping track of the number of points per box. We give each box a weight $p_i(l)$ associated with the number of points it contains by defining

$$p_i(l) = \lim_{N\to\infty} \frac{N_i}{N}$$

where N_i is the number of points in the ith box when we restrict to a randomly chosen subset of N points. We then define the qth moment of the probability distribution,

$$D_q \equiv \frac{1}{q-1} \lim_{l\to 0} \frac{\log \sum_i p_i^q}{\log(l)}$$

where q is any real number. For $q=0$, D_0 is the ordinary fractal dimension defined above. For q large and positive, D_q gives information about the most dense regions of the fractal. For q large and negative, D_q gives information about the least dense regions. Experimentally, we find that D_q is more sensitive to high frequency noise for positive q and to low frequency drifts and finite time series lengths for negative q.

Alternatively we may characterize the variation in density of a set by looking at the local scaling (α) and calculating the dimension (f) of that subset of points which have a given value of the scaling. This function, the *multifractal spectrum*, $f(\alpha)$ encodes all the global scaling information of the set of a compact form [63], [130].

Following the method of Jensen *et al.* [77] we determine the $f(\alpha)$ spectrum as follows: we pick a point x_i in the set and find the density of points, p_i, around it. As in our fractal dimension calculation we may do this by picking boxes of size m and letting $p_i(m) = \lim_{N\to\infty} (N_m/N)$, where N_m is the number of points in the box when we restrict to N points. We may then define α_i by the relation $p_i(m) = m^{\alpha_i(l)}$ in the limit $m\to 0$. Letting $p_i = \lim_{m\to 0} p_i(m)$ we obtain the local scaling at each point. We can now measure the fractal dimension of the set of points with a given value of α by box counting a second time. If we set an acceptance interval $d\alpha$ and let $n(\alpha, l)$ be the number of boxes of side l with $\alpha \in [\alpha_0, \alpha_0 + d\alpha]$, we obtain, in the limit $\alpha\to 0$ and $l\to 0$,

$$n(\alpha, l) = d\alpha \rho(\alpha) l^{-f(\alpha)}$$

where $\rho(\alpha)$ is a smooth function independent of l that does not affect the value of $f(\alpha)$.

Once again, box counting is not the most convenient way to calculate $f(\alpha)$. However, it is the method which makes the meaning of the function most explicit (the $f(\alpha)$ spectrum can also be understood in the context of thermodynamics [42], [132]). In practice one calculates first the generalized dimension and defines a rescaled generalized dimension $\tau(q) \equiv (q-1)D_q$. Then, using the equivalence of dimension and scaling mentioned above, $f(\alpha)$ is the

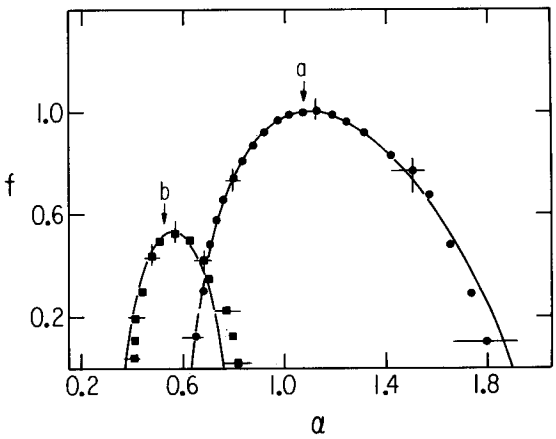

Fig. 6. Multifractals. $f(\alpha)$ curves for (a) the quasi-periodic transition to chaos at the golden mean and (b) the period doubling transition in the 8/13-tongue. Solid lines indicate theoretical calculations for the circle map. Dots and error bars indicate experimental results for small aspect ratio forced Rayleigh–Bénard convection in mercury. From [46] and [77].

Legendre transform of $\tau(q)$ given by

$$\alpha = \frac{d\tau(q)}{dq}$$

and

$$f(\alpha) = \alpha q - \tau(q).$$

Large scaling exponents correspond to low density, so the low α side of the $f(\alpha)$ curve corresponds to positive q and the high α side to negative q. Depending on the system under study different tricks can be used to obtain $\tau(q)$ [46], [47], [62], [63].

For the circle map, $f(\alpha)$ characterizes unambiguously the transition to chaos for both locked and quasi-periodic states. It may either be calculated at $k=1$ for irrational winding numbers or at accumulation points of period doubling cascades inside tongues. In both cases certain landmarks, e.g., the position and value of the maximum of f ($f_{\max} = D$), the smallest and largest α's, the upside-down paraboloid shape of the curve, etc. are extremely robust to minor changes in the map. For example, the period doubling cascades of the logistic map $F(\theta) = k\theta(1-\theta)$ and the sine map produce identical $f(\alpha)$ curves. For theoretical curves see Fig. 6(a) for the quasi-periodic transition and Fig. 6(b) for the period doubling transition.

There is also a hidden bonus for the experimentalist. Below criticality the exact $f(\alpha)$ curve collapses immediately to a point located at $f=1$, $\alpha=1$ for quasi-periodic states and at $f=0$, $\alpha=0$ for periodic states. It does this at irrational winding numbers because, below $k=1$, the map $F(\theta)$ is conjugate to a pure rotation. This means that at very small length scales the Poincaré section looks just like a circle and has uniform dimension equal to 1. There is no interesting scaling. Similarly, below the accumulation point of the period doubling cascade, the Poincaré section consists merely of a finite number of points. Hence at small length scales we see only a discrete set of points of uniform dimension 0. However, an experi-

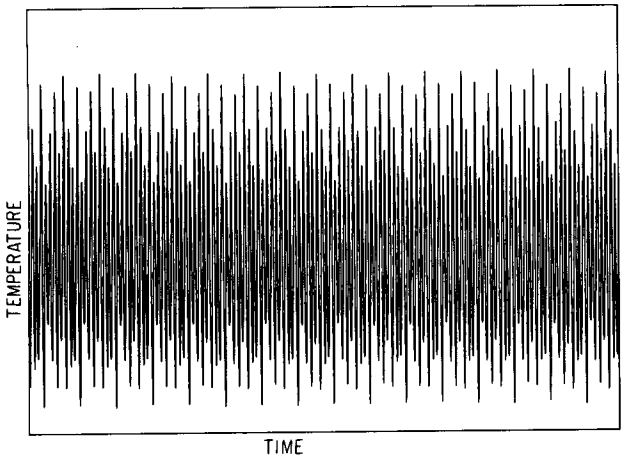

Fig. 7. Experimental time series. An 8/13 locked state for small aspect ratio forced Rayleigh–Bénard convection in mercury. The basic oscillation is the low frequency (f_1) so the blocks contain 8 oscillations. The apparent phase drift is an artifact due to slow sampling rate of the digitization.

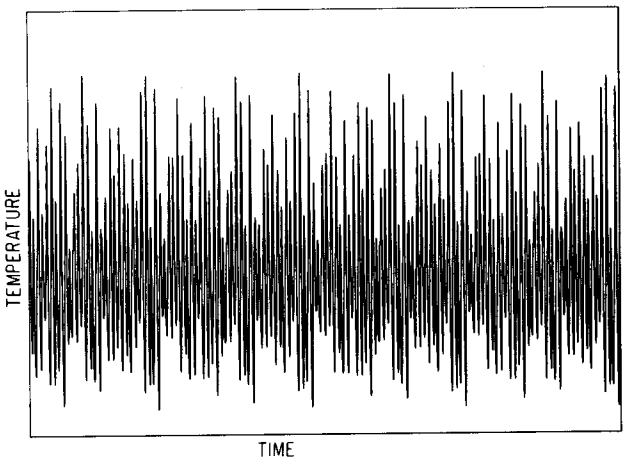

Fig. 8. Experimental time series. A $3 \otimes 34/55$ locked state for small aspect ratio forced Rayleigh–Bénard convection in mercury. The basic period 34/55 and the period tripling envelope modulation are clearly visible. The basic oscillation is the low frequency (f_1) so the blocks contain 34 oscillations.

mentalist has access only to finite length scales because he cannot record an infinite number of points. Thus he will always observe density variations and obtain a nontrivial $f(\alpha)$ spectrum, even much below criticality, as seen in Fig. 10. This is useful for two reasons. 1) He need not worry if his data is taken a little away from the critical point. 2) Arneodo [6] has shown that away from criticality the calculated $f(\alpha)$ curves will narrow in a predictable way as either k is decreased or the number of points used increased. By observing this *Arneodo narrowing* an experimentalist can derive a value of k directly from an experimental time series. This is extremely helpful because the experimental control parameters do not in general correspond exactly to k and Ω and the scaling the Fourier spectrum (discussed below), which is the only other technique for determining the amplitude of the nonlinearity k, is only quantitative at the critical line.

Time Series, Poincaré Sections, and Spectra

To bridge the gap between experiment and theory we must consider the general features of a signal generated by two nonlinear coupled oscillators. We may then ask what the time series of an experiment agreeing with the circle map should look like. We will assume throughout the following discussion that $f_2 > f_1$, however, the same arguments will hold in the opposite case. The time series will show a more or less sinusoidal oscillation at the natural frequency f_1. The second frequency f_2 will produce a beat pattern superimposed on this basic oscillation. In a locked state, $f_1/f_2 = p/q$, we will see a repeated unit block composed of p fundamental oscillations. We show an experimentally observed 8/13 signal in Fig. 7. A period doubling will appear as a second modulation with period $2p$, making the amplitude of the blocks alternately large and small. As mentioned previously, the period doubling does not change the winding number. It takes $p/q \rightarrow 2p/2q$. A general period multiplication by n of a state p/q, will result in a periodic time series $(n \otimes p/q)$ with a period np/f_1. We show another experimentally observed state of form $3 \otimes 34/55$ in Fig. 8. The basic period 34 (the time series showing the numerator of the fraction) and the period tripling envelope modulation are clearly visible. A quasi-periodic state will look similar, except that the envelope will gradually drift in phase with respect to the fundamental oscillation. Chaotic states have additional irregular modulations. The attractors of weakly chaotic quasi-periodic states are nearly impossible to distinguish from ordinary quasi-periodic attractors. However, chaotic period doubled attractors are clearly distinguishable from ordinary locked states, showing smeared pointlike attractors which may drift to such an extent that they fill the entire circle.

In applying the above model to a real experiment, we must take into account the conflicting effects of noise. On the one hand, we can never achieve a true quasi-periodic state, since we cannot set the winding number exactly, and the external frequency inevitably varies slightly in time. The system will always tend to lock since the presence of even an arbitrarily small amount of noise will shift a quasi-periodic state to a nearby locked state. On the other hand, noise also smears out high denominator tongues. We may think of each tongue as a potential well whose depth varies inversely with the denominator of the tongue. In the presence of noise the state can tunnel between nearby tongues of high denominator. The system will not remain in a given large denominator tongue for an arbitrarily long time. Thus when we speak of an experimental quasi-periodic state, we mean only that we cannot measure any true periodicity over the duration of the experiment. Another limitation is that for a finite measurement time we cannot distinguish arbitrarily low frequencies. For a true quasi-periodic state with $W = \sigma$, all of the $\{\sigma_i\}$ will be approximate periods. For some value of i our experiment will fail to distinguish the difference between σ_i and σ_{i+1}. This is the limiting resolution of the experiment [46], [125]. Because the golden mean is furthest from rationals of any

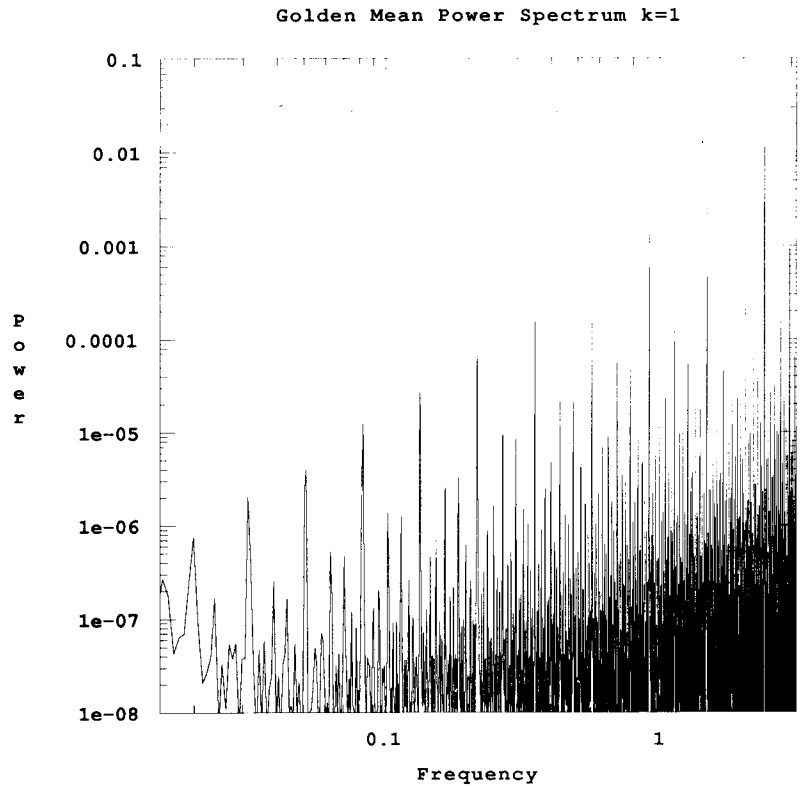

Fig. 9. Power spectrum for the critical golden mean circle map. The series of large peaks are at frequencies σ_G^n. The pattern of peaks between each pair of main peaks is the same and the envelope of the peak heights goes as ω^2.

given denominator, it is the irrational winding number most resistant to noise. A golden mean state can be knocked further without locking to a low denominator tongue.

Using time series alone, it is rather difficult to distinguish quasi-periodic states from chaotic states arising from quasi-periodicity. The power spectrum:

$$P(\omega) = \left| \frac{1}{2\pi} \int dt f(\theta) e^{2\pi i \omega t} \right|^2$$

provides an immediate indication, however, and is not sensitive to random variations in winding number. If two oscillators of frequencies f_1 and f_2 are coupled nonlinearly, all frequencies of form $f_{n,m} \equiv nf_1 + mf_2$ (where n and m are integers) will be present in the power spectrum, with the amplitude of the peaks decreasing rapidly with increasing m and n. Surprisingly, going from a continuous system to the circle map does not affect the global properties of the spectrum. It merely sets $f_2 = 1$. We may define the power spectrum for the discrete series as

$$P(\omega) = \lim_{i \to \infty} \left| \frac{1}{q_i} \sum_{j=0}^{q_i - 1} \theta_j e^{2\pi i \omega j} \right|^2$$

where q_i is the denominator of σ_i. For periodic states the number of distinct $f_{n,m} \leqslant f_1$ is just p, the lowest frequency being f_1/p and the low frequency spectrum will consist of a finite number of lines of form jf_1/p. If the system is quasi-periodic, however, the $f_{n,m}$ are distinct for all n and m and the spectrum will consist of a countable infinity of lines. The combination frequencies are particularly well behaved at the golden and silver means. Because the golden mean has the property that its nth power $\sigma_G^n = F_{n-1} - \sigma_G F_n$, all powers of the golden mean are linear combinations of the fundamental frequencies and hence will be present. If we plot the low frequency part of a golden mean spectrum on a log scale, as shown in Fig. 9, we obtain a set of equally spaced peaks at frequencies $\sigma_G, \sigma_G^2, \sigma_G^3, \cdots$ [32], [106], [118]. There are also smaller amplitude sequences of peaks at frequencies, $\{\sigma_G^n(\sigma_G + m)\}$ which lie between the main peaks. The silver mean behaves identically, substituting σ_S for σ_G. The pattern of the peaks is self similar, that is, the pattern between, for example, σ_G^3 and σ_G^4 is identical, up to scale factors in frequency and amplitude, to the pattern between σ_G^6 and σ_G^7 as can be seen in Fig. 9.

We may use the amplitude of the combination peaks to estimate k. For $k < 1$ the amplitude of these peaks drops off exponentially with m and n resulting in a clean spectrum with a finite number of measurable lines, as seen in Fig. 10 (a2) and (b2). However, at $k = 1$ the amplitude of each series drops off algebraically, $P(\sigma_G^n) \sim \sigma_G^{2n}$ as can be seen in Fig. 9 and Fig. 10 (c2). If we divide by ω^2 to define the normalized power spectrum, $P(\omega)/\omega^2$, its envelope remains flat as $\omega \to 0$. Finding the power of ω that yields a flat envelope and counting the number of visible combination peaks, gives a qualitative estimate of k. The lower the power of ω and the more combination peaks are visible, the closer the state is to criticality.

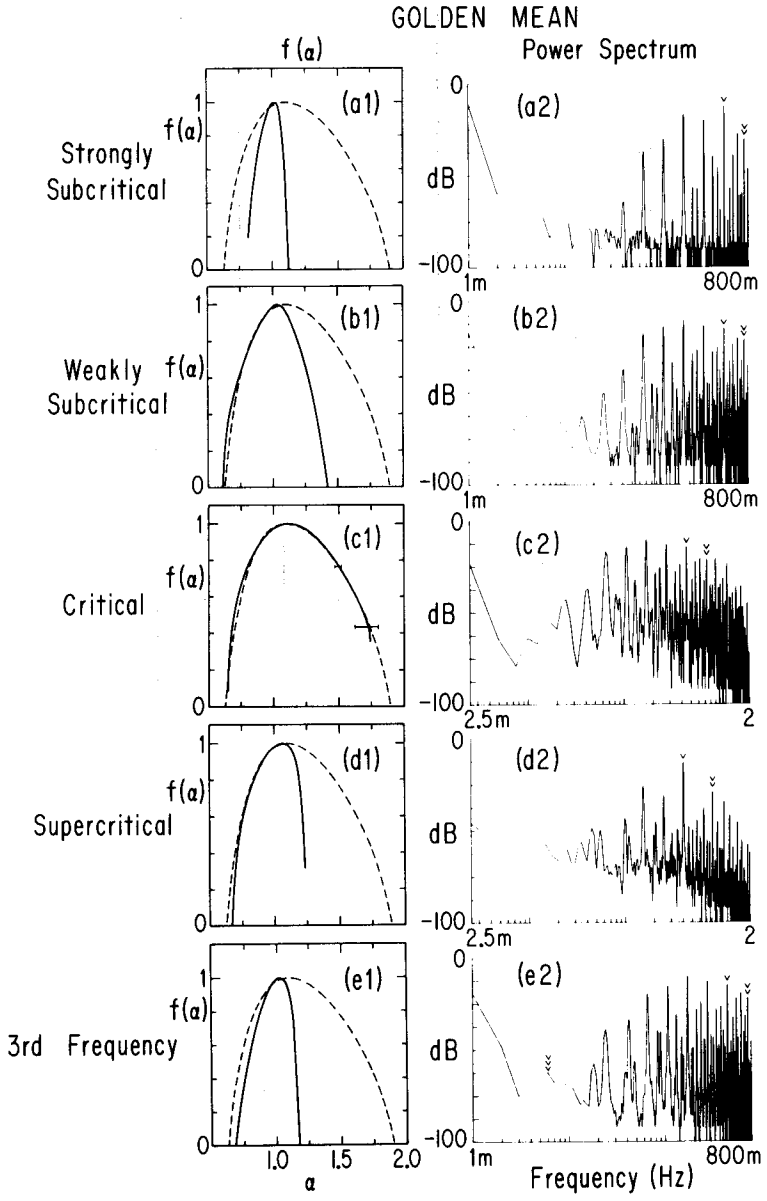

Fig. 10. Experimental Spectra and $f(\alpha)$ curves for small aspect ratio forced Rayleigh–Bénard convection in mercury: Column 1, golden mean $f(\alpha)$ curves (dashed lines show the numerically calculated critical curve); column 2, golden mean spectra. Row a, strongly subcritical; row b, slightly subcritical; row c, critical; row d, supercritical; row e, third frequency present. In column 2 single arrows mark the frequency of the oscillatory instability (f_{int}), double arrows the forcing frequency (f_{ext}). In (e2) triple arrows mark the third frequency. The number of points used to calculate the $f(\alpha)$ curves were: (a1), 89; (b1), 144; (c1), 377; (d1), 383; (e1), 123. The equivalent Arneodo couplings are: (a1), $k = 0.960$; (b1), $k = 0.977$; (c1), $k = 0.995$. Note the $1/\omega^2$ scaling in (c2). The error bars indicated in (c1) and (c3) are maximal deviations. For other figures the errors are typically a few percent. From [47].

Above $k = 1$ there are chaotic and period multiplied states. The nth period doubling appears as a subharmonic at $f_1/2^n$. In general any multiplication of period by m will appear in the form of mth subharmonics, $m-1$ peaks between each of the main combination peaks. Chaotic states are qualitatively different from those discussed above. Their aperiodicity does not result from combinations of well defined incommensurate frequencies but from the presence of a $1/f$-like continuum of low frequencies. These frequencies produce broadband noise throughout the spectrum. The noise increases in amplitude with k, gradually swallowing the quasi-periodic combination peaks and, for large k, resulting in a nearly smooth spectrum.

We must also consider noncircle map effects. A complex experimental system can only resemble the simple circle map when all but one degree of freedom in its motion is suppressed. For small perturbations this suppression is not surprising, but for large external perturbations we expect that we may excite additional degrees of freedom, raising the system's effective dimension [17]. One symptom of an increase in dimensionality is wrinkling of the Poincaré section—that is, the Poincaré section folding up on itself to form a fractal with dimension between 1 and 2. As long as the wrinkling is small and the dimension is close to 1 our simple circle map will be a reasonable approximation. However, for very strong forcing, the Poincaré section

tends to dissolve into a gnatlike sea of points and the dimension approaches two [47]. In this case we need to embed our system in a higher dimensional space and use a higher dimensional model like the Henon or Standard maps [5]. Two-dimensional extensions of the circle-map, like the dissipative Standard map:

$$\begin{pmatrix} \theta_{i+1} \\ x_{i+1} \end{pmatrix} = \begin{pmatrix} \theta_i + \Omega - \dfrac{k}{2\pi}\sin(\theta_i) + \epsilon x_i \\ \epsilon x_i - \dfrac{k}{2\pi}\sin(\theta_i) \end{pmatrix}$$

are particularly appealing since they can be reduced continuously to the one-dimensional case. Unfortunately, if it is difficult to determine k experimentally, it is nearly impossible to determine ϵ. Experimental and theoretical techniques exist to treat this case but they are much less well developed than those for the simple circle map. We will discuss two dimensional effects briefly in the experimental section of this paper.

IV. Experimental Results

Now that we know what to look for we may examine the experimental evidence. We will limit our discussion to frequency locking effects and neglect the related one-dimensional mapping problems of phase locking and simple period doubling. We have studied quasi-periodic effects in small aspect ratio forced Rayleigh–Bénard convection [46]–[48], [77], [123], [124], and we will describe this system in detail. A large range of effects have also been observed in oscillations in Germanium [61], [62], [69]–[71]. We will discuss other experimental results when relevant. Experiments on quasi-periodicity fall into two broad classes, those in which the frequency f_2 is externally controlled (which we will denote *type I*, and those in which it arises internally, which we will denote *type II*. Experiments of type I allow much greater control over the varieties of quasi-periodic behavior observed and we will concentrate on them.

Forced Rayleigh–Bénard Convection

Our Rayleigh–Bénard convection experiment consists of a small mercury-filled rectangular cell ($1.4\times0.7\times0.7$ cm^3) with plexiglass walls and copper plates on the top and bottom. The cell has its temperature regulated to a few thousandths of a degree celsius and is placed in a horizontal magnetic field of ≈ 200 G aligned perpendicular to its long axis. We begin with a motionless fluid and heat the cell from below. The heating causes the fluid at the bottom of the cell to expand and lose density. At a few degrees temperature difference the inverted density gradient becomes unstable and the hot and cold fluids exchange places (convect) forming horizontal, time independent rolls. The magnetic field acts to damp motion perpendicular to its axis and aligns the convective rolls parallel to the short side of the cell. If we increase the heating further, to about 10°C, the rolls themselves become unstable to the *oscillatory instability* and begin to oscillate transverse to their axes. Further increasing the heating results in the appearance of additional low frequencies which have been used to observe type II frequency locking effects [49], [84]. Other fluids with different thermal properties show different sequences of instabilities but the basic sequence: motionless, steady motion, periodic oscillation, and finally, multiperiod oscillation, is the same. The oscillatory instability produces a well defined frequency (defining f_1) which depends on the box size, magnetic field strength and temperature difference. In the experiments to be discussed, f_1 is typically between 0.2 and 0.4 Hz. We then inject an alternating pulsed current sheet (frequency f_2 and amplitude A) asymmetrically through the mercury. The current and magnetic field produce an alternating Lorentz force which couples nonlinearly to the oscillations of the rolls [124]. The whole procedure closely resembles stirring a pot of soup while heating it on a stove.

The experimental control parameters related to the nonlinearity are the amplitude of the current pulses (A) and their duty cycle (x). If the total forcing power (xA^2) is too large, it can drive the oscillatory instability off resonance and suppress it. Since the amplitude of the nonlinearity depends on the product of the internal and external oscillator amplitudes, and is more sensitive to peak height than power (it goes roughly as xA), we use narrow δ-function pulses to reach the maximum possible nonlinearity without killing the internal oscillation.

We measure the temperature of the system at the center of the bottom of the cell using a semiconductor bolometer. A very useful theorem proposed by Poincaré and proved by Takens and Swinney [120], [128], [131] assures that as long as the flow in the cell is coherent (i.e., the flow is not turbulent) all information about the cell behavior can be reconstructed from any local measurement of any system variable.

In the first set of experiments we scanned the A, f_2 plane to map the locking behavior. We present the results in Fig. 4. We found excellent agreement with the standard Arnol'd structure with no duplicated or missing winding numbers and the correct qualitative tongue widths. We then located the position of the critical line at σ_G and σ_S (here defined as the A value at which broadband noise first appears in the spectrum) and calculated the scaling exponent δ and the approximate fractal dimension of the quasi-periodic structure D' by explicitly measuring the widths of tongues in the "best" approximant series with a denominator of 100 or less, as shown in Fig. 4. We obtain: $\delta_{\sigma_G} = 7.0 \pm 10\%$, $\delta_{\sigma_S} = 2.8 \pm 10\%$, and $D' = 0.86 \pm 3\%$ for both winding numbers. This agrees with the theoretical predictions discussed earlier and supports the hypothesis that the fractal dimension of the set of quasi-periodic winding numbers at criticality is uniform. However, the critical line is by no means straight, indicating that the correspondence between A and k is only approximate. Together these results establish the global similarity between forced Rayleigh–Bénard convection and the simple circle map. We have also, by means of a three-dimensional Poincaré section (T_i, T_{i+1}, T_{i+2}), been able to untangle the

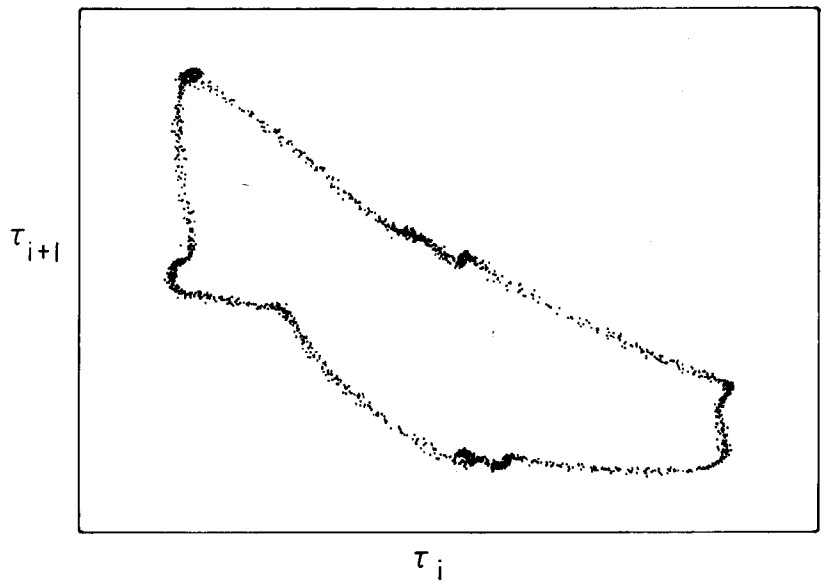

Fig. 11. Experimental critical attractor for small aspect ratio forced Rayleigh–Bénard convection in mercury. The attractor is wrinkled, indicating two dimensional effects, and varies in density. The width of the attractor results from temperature drift in the experiment. From [125].

attractors and calculate the return map $F(\theta)$ explicitly from the experimental data [124]. We present three-dimensional Poincaré sections and unwindings for weak, moderate and critical forcing in Fig. 11. In each case the resulting curve is clearly one dimensional, justifying the circle map model.

We next examined the nature of the transition to chaos at σ_G and σ_S. The experimental procedure consisted of selecting a winding number σ and then, for each change of the forcing amplitude, approximating it to the desired accuracy by adjusting the forcing frequency to lock successively to each of the best approximants $\{\sigma_i'\}$. By directly examining the periodicity of the locked time series we could rapidly tune the winding number to 5 parts in 10^6, since tongues with denominators up to around 1000 are stable. One problem is the low basic frequency of the system, which results in long data acquisition times and sensitivity to long term temperature drift.

Fein, Heutmaker, and Gollub made the first experimental observation of the golden mean critical power spectrum in a hydrodynamic system. They studied forced Rayleigh–Bénard convection in water using a $2.1\times1.6\times0.8$-cm^3 cell driven by thermal pulses and detected density gradients in the fluid using optical techniques. Drifts and pattern competition instabilities prevented them from tuning their frequency ratio to better than 1 part in 10^3. Nevertheless, they were able to observe a roughly self-similar spectrum with ω^4 scaling of the peak heights [41]. Our work on spectra has confirmed and amplified those results. If we examine spectra at the golden and silver means we find the predicted pattern: well defined line spectra below criticality, power law (ω^2) scaling at criticality and broadband noise above [47], [123]. We present subcritical spectra in Fig. 10 (a2) and (b2), critical spectra in Fig. 10 (c2), a rescaled critical spectrum in Fig. 12, and supercritical spectra in Fig. 10 (d2), all at the golden mean. We have calculated the $f(\alpha)$ spectrum below, at, and above criticality for both σ_G and σ_S and find excellent agreement with theoretical predictions. We present golden mean results in Fig. 10 (a1)–(d1) and Fig. 6(a). We find good agreement with the predicted Arneodo narrowing for subcritical $f(\alpha)$ curves, and are able to use it to calculate k. We have also examined the effects of a third frequency on the spectrum and critical $f(\alpha)$ curve and find adequate agreement with theoretical predictions. We present these results in Fig. 10 (e1) and (e2).

The agreement between the experiment and circle map is surprising. Indeed it is so good one might wonder if the system were not simply a slow analogue computer simulating the circle map. Fortunately things are not that simple. We know that for very strong forcing we have turbulent (high-dimensional) behavior. These extra dimensions must begin to make themselves felt at some point. In practice, the first sign of the breakdown of sine map behavior is the wrinkling of the Poincaré section which begins near criticality as seen in Fig. 13. Just above criticality the dimension of the attractor creeps above 1, and 10% above, the attractor has exploded into a full two-dimensional set.

If we look for period doublings inside a tongue we see higher dimensional behavior of a different kind [46]. The doubled attractors themselves are unsurprising. In Fig. 14 we show Poincaré sections of a pure 8/13 state and a triply period doubled, $2^3\otimes 8/13$ state. The periodic attractors have nearly the same shape as the quasi-periodic attractor shown in Fig. 13, indicating that the form of the torus is independent of the trajectory. This agreement is an example of universality that would be difficult to explain outside the context of dynamical systems theory. However, the sequence of multificurcations within the tongues is not that predicted by the one dimensional model. We have mapped the 8/13 tongue in detail and present it in Fig. 15. At the edge of the tongue and for small nonlinearities the

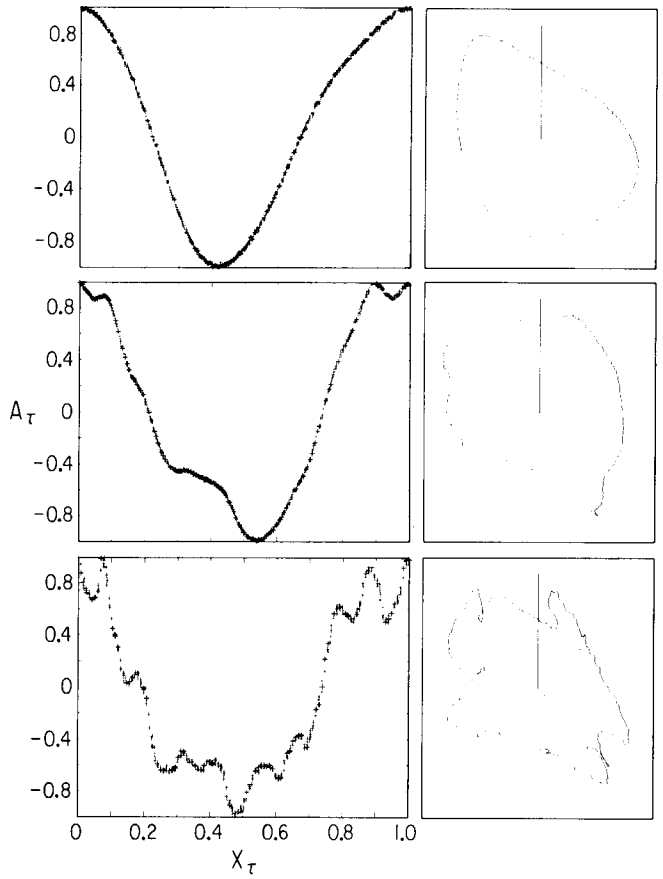

Fig. 12. Three-dimensional Poincaré sections and unwindings of experimental golden mean time series for small aspect ratio forced Rayleigh–Bénard convection in mercury. Column 1 shows the one dimensional unwinding described in the text. Column 2 shows the three dimensional Poincaré section. The top section shows weak forcing, the middle moderate and the bottom critical. From [124].

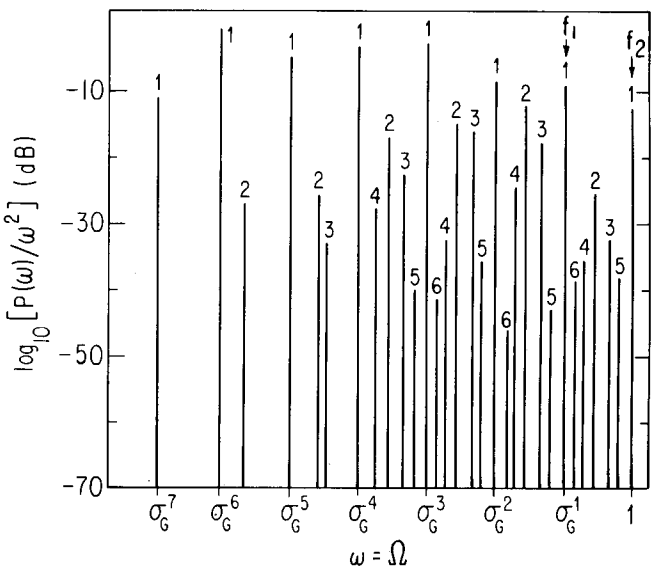

Fig. 13. Rescaled experimental critical spectrum at the golden mean for small aspect forced Rayleigh–Bénard convection in mercury. Only the first few series of peaks are shown. The envelope is flat for all series, indicating ω^2 critical scaling. From [123].

structure is still largely one dimensional. The overlapping of neighboring tongues is that predicted by the one dimensional circle map, as are the various intermittency effects [126]. The first period doubling occurs slightly above criticality, and according to the one-dimensional scheme of Glass and Perez [13], [107]. We also observe the predicted symmetry breaking bifurcation (that is there are two distinct types of period 4 cycles), followed by period doubling cascades at the sides of the tongue. We have measured the $f(\alpha)$ curve for one of these cascades and find excellent agreement with that predicted for simple period doubling, as seen in Fig. 6(b). So far this is normal one dimensional behavior. However, when we move towards the axis of the tongue, the situation changes. Instead of the predicted pure period doubling cascade, we find paired "bells" of odd subharmonics, with the order of the subharmonic increasing toward the tongue axis. Inside each of these subharmonic bells we observe a subsidiary period doubling cascade. That is, proceeding from tongue edge to center, we find $2^n \otimes \frac{8}{13}, 2^n \otimes 3 \otimes \frac{8}{13}, 2^n \otimes 5 \otimes \frac{8}{13}, \cdots$. We are able to observe subharmonics up to 13 but have only succeeded in mapping up to 5. Furthermore these subharmonic bells overlap, leading to a strongly hysteretic multisheeted structure in which states of form $m \otimes \frac{8}{13}, n \otimes \frac{8}{13}$, and $m \otimes n \otimes \frac{8}{13}$ can all exist for the same values of A and f_2. The simple circle map predicts no hysteresis in these regions. There are also various two-dimensional intermittency effects resulting from noise induced jumps between sheets within the tongue.

At first this structure seems completely incomprehensible in terms of the circle map model. However, similar, though not identical, structures have been predicted and more recently calculated for various two dimensional maps by MacKay and Tresser [89]–[91], [134]. We may understand this mixture of one- and two-dimensional behavior by considering the nature of a locked state. Near the edge of the tongue the system is detuned, resulting in a relatively large damping (effectively the nonlinearity is smaller near the edge of a tongue). As we move toward the center of the tongue and the resonance condition, the damping decreases, allowing the normally suppressed second dimension to appear. Taking the dissipative standard map as an example, we might say that $\epsilon = 0$ at the edge of the tongue and increases to a maximum on the tongue axis. In this case the sequence in which the subharmonics appear should allow calculation of ϵ as a function of the distance from the tongue axis.

Recently, Ecke and Haucke have succeeded in observing a similar range of phenomena, including well-defined Arnol'd tongues and period doubling, as well as a variety of three frequency states in binary convection in a ^{3}He-superfluid ^{4}He mixture [67], [68], [35], [66], [64]. Their system contains two internal frequencies whose ratio is precisely controlled by varying the Rayleigh number.

Thus in the simple convection experiments, it is possible to produce the full range of circle map behavior and to introduce higher dimensional effects in a controlled fashion. This holds out the hope that we can treat more complex hydrodynamic systems using extensions of the simple theory, rather than having to start from scratch.

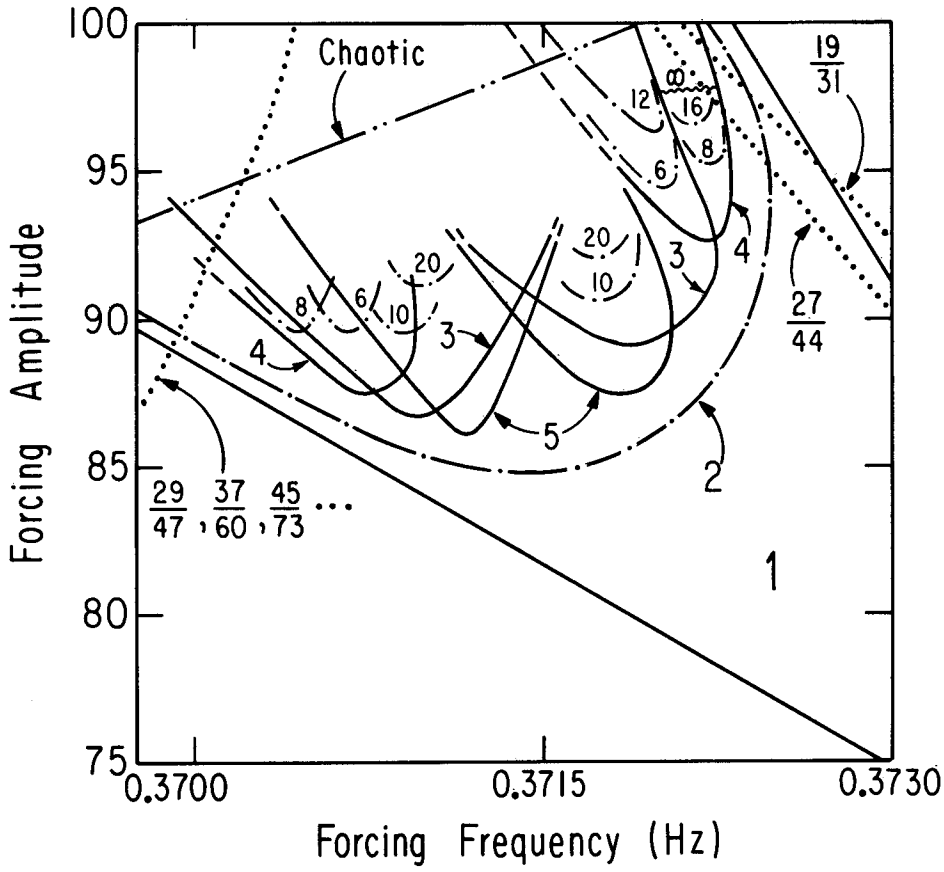

Fig. 14. Subharmonic structure of a tongue in small aspect ratio forced Rayleigh–Bénard convection in mercury. The 8/13-tongue is shown in the A versus Ω plane. The lines inside the tongue indicate the borders between different periodic states. Overlaps indicate regions of multistability. The areas labelled by n correspond to $n \otimes 8/13$ states. The single dotted lines indicate smooth period doubling transitions. The solid lines indicate discontinuous transitions. The dotted lines on the right and left hand sides of the tongue indicate the position of overlapping tongues. The double dashed line indicates the region where the system is chaotic for all forcing frequencies. Note the symmetry breaking which follows the first period doubling and the sequence of subharmonics. Compare Fig. 5. From [46].

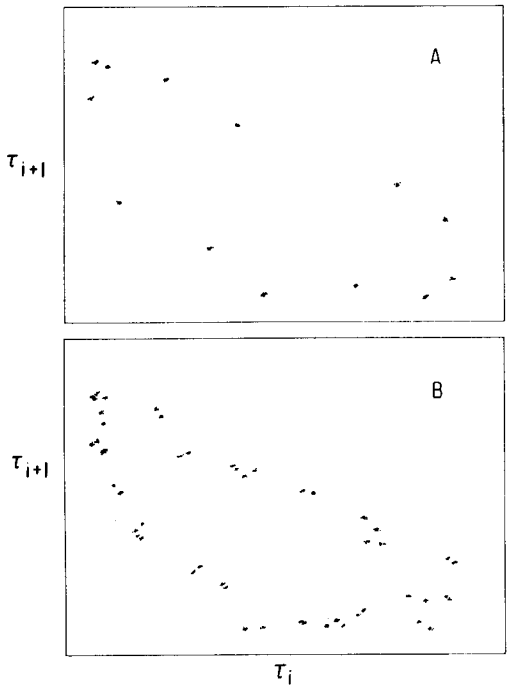

Fig. 15. Experimental Poincaré sections in the 8/13-tongue for small aspect ratio forced Rayleigh–Bénard convection in mercury. (a) A pure 8/13 state. (b) A $2^3 \otimes 8/13$ state. The overall shape of the attractor is the same as in Fig. 11. From [46].

Solid-State Systems

Of the numerous solid state systems exhibiting quasi-periodic behavior, electrically forced germanium is the most studied. In the experiment of Held and Jeffries [70], [72] a single crystal (1 mm^3) of n-type germanium with a electron injecting contact made of diffused lithium and a hole injecting contact of diffused boron, is cooled to liquid nitrogen temperatures. When the crystal is subject to a dc electric field (15.02 V) and magnetic field (9.32 kG) it produces measurable oscillations in the form of traveling density waves in the electron-hole plasma. The typical frequency is 235 kHz which makes data acquisition somewhat inconvenient. Depending on the angle between the magnetic and electric fields and their relative amplitudes, the system can oscillate at either one or many frequencies (resulting in type II frequency locking [69]). However, in the experiment, the angle and drive voltage were adjusted to produce a single well defined f_1, and an alternating voltage was applied between the contacts to define f_2. The measured variable was the total current through the sample $I(t)$.

They found the standard Arnol'd tongue structure with the fractal dimension for the unlocked set at the critical line being $D' = 0.90 \pm 0.03$ and the scaling $\delta_{\sigma_G} = 2.7 \pm 0.5$

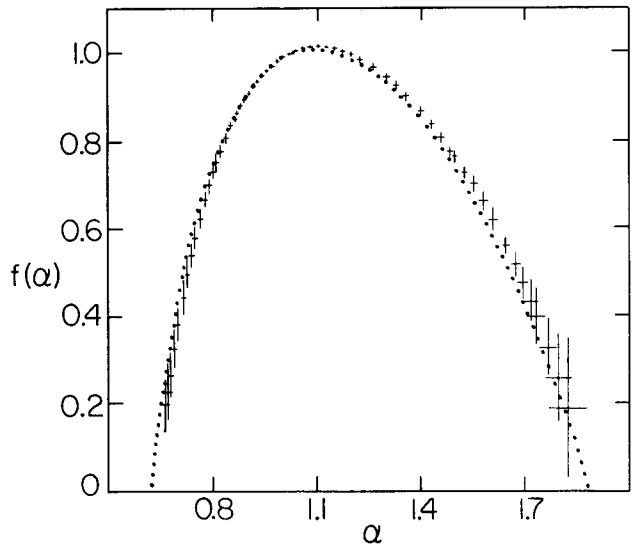

Fig. 16. Multifractal spectrum at the critical golden mean in electrically forced germanium. The solid line is the theoretical curve for the circle map. Dots and error bars are the experimental results. The high accuracy for large α (low densities) is remarkable. From [62].

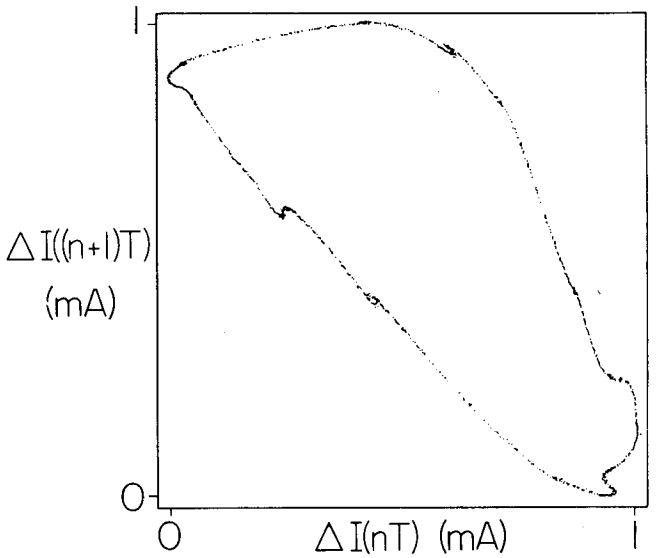

Fig. 17. Experimental attractor at the critical golden mean in electrically forced germanium. The attractor is wrinkled, indicating the presence of two-dimensional effects. From [62].

in agreement with the simple sine map. The power spectrum at the golden mean shows the expected behavior and critical (ω^2) scaling. Unlike the Rayleigh–Bénard attractor, the germanium attractor does not wrinkle or explode until well above the transition to chaos [72]. They have also examined forcing at two incommensurate external frequencies and found three frequency quasi-periodicity with frequency locking to either forcing frequency. There is a well defined critical surface in agreement with the predictions of Ostlund, Kim and Siggia [55], [79], [80], [106]. Unfortunately their signal-to-noise ratio was not sufficient to allow them to map a three frequency tongue in detail.

Gwinn and Westervelt [61], [62] have performed a similar experiment on oscillating electric field domains, using cooled (4°C) germanium with boron implanted contacts. They applied a dc bias to induce oscillations at roughly 10 kHz and superimposed an ac driving voltage. The measured quantity was $I(t)$. They observe the expected Arnol'd diagram with ω^2 power spectrum scaling at the golden mean. Their calculations of $f(\alpha)$ at the critical golden mean are in excellent agreement with those for the circle map. We reproduce their $f(\alpha)$ curve from [62] in Fig. 16. The high accuracy they obtain for large α is particularly impressive, since these are measurements made where the attractor density is lowest and hence require long time series and good stability. Their attractor (Fig. 17) shows clear signs of wrinkling at criticality but is otherwise extremely clean.

Martin and Martienssen [93], [94] have obtained a very clean circle-map-like return map and devil's staircase behavior in electrically driven Barium Sodium Niobate at high temperatures (500°C). Because of temperature drift problems their Poincaré sections are limited to about 500 points. They observe a standard Arnol'd diagram but are limited to denominators <10. Zettl and Grüner have obtained a nearly complete devil's staircase and incomplete period doubling cascades in forced charge density waves in $NbSe_3$ [22], [57]. They obtain a fractal dimension for the unlocked set at the critical line of $D = 0.91 \pm 0.03$. Other groups have obtained similar results in a variety of charge density wave systems [88].

Winful, Chen, and Liu [138] have observed frequency locking behavior in a periodically forced semiconductor laser. An internal instability in their AlGaAs/GaAs laser generates f_1 at a frequency between 0.5 and 3 GHz, and an externally applied RF modulation at a lower frequency defines f_2. For weak forcing they obtained a standard Arnol'd tongues diagram with appropriate tongue widths. They are able to follow the golden and silver mean quasi-periodic states over a wide range of forcing amplitudes, and to observe the expected transition from line spectra to broad band noise at criticality. Unfortunately the extremely high frequencies limit their signal-to-noise ratio to 40 dB, so they are unable to resolve more than the first few combination peaks or to tune their frequency ratio to better than 1 percent. For large forcing amplitudes (well above the onset of chaos) they observe a complicated pattern of disappearing tongues without period doubling. This behavior is typically two dimensional, and they provide a two dimensional differential equation model to explain it.

That such a variety of natural systems exhibit behavior quantitatively identical to the one-dimensional circle map is one of the great successes of dynamical systems theory.

Analogue Simulators

Another category of type I system is the nonlinear electronic circuit specifically built to exhibit quasi-periodic behavior. Bryant and Jeffries [23], [24] have studied a system incorporating a magnetic inductor with hysteresis. The system exhibits frequency locking and Arnol'd tongues,

however its behavior is complicated. The ordering of the tongues is not that of the simple circle map. There are missing and extra tongues with unexpected widths. There is no well defined critical line and subcritical tongues overlap. The period doubling behavior within the tongues is also anomalous, without any apparent symmetry breaking. The data recalls that of many two dimensional systems of differential equations [8], and Bryant and Jeffries provide a multidimensional model. Gollub *et al.* [51] have observed similar complicated locking behavior in tunnel diode circuits. We will not describe here the numerous other experiments in electronic systems built purposely to emulate circle map type behavior [25], [75], [86], [109], [133].

Recently, Su, Rollins, and Hunt [127], and Cumming and Linsay [31], have measured $f(\alpha)$ curves for analog simulators. Su, Rollins, and Hunt employed coupled diode-inductor resonators, Cumming and Linsay, a more complicated analog circuit. Both obtain reasonable agreement with the predictions of the circle map, though the results of Cummings and Linsay show anomalous behaviors apparently due to discontinuities in the return map describing their system.

How one judges analogue simulators is a philosophical problem. They have the advantage that they can be described by ordinary differential equations and thus simulated on a computer, but their relevance to dynamical systems theory is less clear. A dynamical systems approach is most valuable for systems like convection, which cannot be solved exactly. It is somewhat ironic that the simple theory works best in intractably complex continuous systems, and fails badly in simple simulators.

Multiple Internal Frequency Quasi-Periodicity

We can only mention a few of the many experiments done on type II systems. The problem with these systems is that it is difficult to predict whether changing a given parameter will affect both oscillators in the same way. One cannot tune the frequency ratio without affecting the strength of the nonlinearity. Trying to scan a two parameter phase space with one control parameter is a bit like moving in a maze. One can move further or backward but one cannot choose a direction. Nevertheless, in the cleanest of these systems varying a single control parameter results in a well defined sequence of periodic, quasi-periodic and chaotic states. In many cases the return map can also be determined. The typical signature of a circle-map-like system is a well behaved "Devil's Staircase," followed by period doubling cascades and windows of periodicity [12]. Full zoologies have been observed by Maurer and Libchaber in liquid helium [85], [95], [96] and Swinney *et al.* in both chemical (Belousov–Zhabotinsky reaction) and various hydrodynamic systems [52], [135]. In the latter they have obtained $D' = 0.87 \pm 0.02$ (Couette flow) [129] and attractor blowup above the onset of chaos (channel flow) [20]. Gollub and Benson have observed a similar variety of effects including three frequency quasi-periodicity in unforced small aspect ratio Rayleigh–Bénard convection in water [49]. Three frequency quasi-periodic states and more or less complete Devil's staircases have also been observed in CO_2 lasers [16], [100], and Devil's staircases and other quasi-periodic effects in Fabry–Perot interferometers [4], [98], mechanical systems [34], [60], [101], Josephson junctions [105], and yttrium iron garnet oscillators [1], [44]. Braun *et al.* in plasmas [21] and Keolian *et al.* in the Faraday experiment [78] have found mixed period doubling-subharmonic cascades similar to those observed in our forced Rayleigh–Bénard convection experiment. In general the numerical accuracy of type II experiments is much lower than in the type I systems described above, so these results serve chiefly to confirm the large range of validity of the one-dimensional circle map model.

IV. Conclusions and the Future

The great accomplishment of dynamical systems theory and experiment has been to establish that the same basic description of behavior can apply to a wide range of systems. This universal behavior is independent of the detailed structure which gives rise to it. The same language can describe both Josephson junctions and slime moulds. To return to our computer metaphor: We have indeed developed a machine independent code, and without having had to learn machine language! The recognition of universality in behavior is a tremendous advance in the way we think about complex systems. It tells us what sorts of behavior we can expect from unknown systems, and what questions to ask to establish the class to which a system belongs. However, in its present state, dynamical systems theory is incomplete, both as a technical and as a theoretical tool.

Even in the study of one-dimensional systems the techniques of data analysis are cumbersome. We need more convenient and reliable ways to determine important quantities. The measurement of dimension is now a standard technique. We need to be able to determine winding numbers, $f(\alpha)$ curves, nonlinearity strengths and scaling parameters automatically. Only when making these calculations is as simple as taking a Fourier spectrum will the dynamical systems approach achieve its true potential as a tool for the study of systems. Recent work by Farmer and Sidorowich [39], [40], and Kosterlich and Yorke [81] on the extrapolation of chaotic time series is an excellent example of the type of tools that need to be developed.

Dynamical systems theory, though beautiful mathematically, is chiefly valuable to an experimentalist as an analytical technique. One thinks of basic quantum mechanics as an analogy. One does not, except in a few specialized cases, do experiments to check the basic mechanics of the quantum theory. Instead one uses it to analyze systems that are interesting in their own right. Similarly, with time, model dynamical systems will become less and less important. Once we know that many systems behave like a circle map, finding additional circle-map-like systems becomes less interesting.

We finish by listing, in approximate order of difficulty a few of the remaining problems which dynamical systems theory would need to solve to become a useful theory for explaining the real world: noise is present in all real systems, yet dynamical systems theory is essentially deterministic. We might expect that as systems become noisier the dynamical systems approach will be less relevant. This is not necessarily true, and there has been some progress on a theory of noisy dynamical systems [29], [30], [119]. However, the work of Stratonovich [126] which predates dynamical systems theory by twenty years, remains the most complete treatment of noisy systems. A complete theory of the significance of noise does not exist and experimental work is just beginning [19], [65], [40].

Most natural systems contain more than two frequencies. The behavior of systems with three frequencies is still poorly understood. It is not even known whether there are universal three frequency behaviors. The theoretical predictions concerning three frequency systems are vague and apparently contradictory [55], [103], [110], [115]. There has been some preliminary experimental research but the parameter space in a three frequency problem is huge, and without theoretical guidance it is easy for the experimentalist to lose his way [16], [47], [72].

The theory we have developed works only near the transition to chaos. Even in few dimensions, strongly chaotic attractors are still not well understood, though there has been some recent progress in pushing above the critical line (for example, in analyzing intermittency effects caused by the overlapping of locked tongues [48], [59]).

There is still no satisfactory general theory for many dimensional systems, though there has been significant recent progress toward extending the theory of symbolic dynamics, from the circle map to its two dimensional analogues [5], [9], [17], [59]. The hope has always been that dynamical systems theory could be extended in a consistent fashion dimension by dimension, but preliminary results indicate that the universality of two-dimensional systems is weaker than in the one-dimensional case.

Will it be possible to extend dynamical systems to higher dimensions? Will universality disappear completely in three or more dimensions? Barring such catastrophies, it is clear that any general theory will be significantly more complex than that for one-dimension. One thinks of the extension of simple quantum mechanics to field theory and beyond. For the experimentalist the problems are similarly daunting. We do not know what quantities are of interest, and the data sets required to analyze even two-dimensional systems are enormous. More significantly, most experiments lack a sufficient number of control parameters to explore a many dimensional parameter space fully. It seems that all many degree of freedom systems will be type II and hence hard to interpret. Large systems have a further problem, they tend to develop complex spatial as well as temporal behavior. The measurement of a single variable no longer fully describes the system, and instrumentation and data collection become significant problems. Spatio-temporal chaos is an almost untouched subject. Even Rayleigh–Bénard experiments in wide cells are not understood [14], [50], let alone more complicated natural systems.

The problems are considerable, but the potential payoffs is a deep understanding of a range of natural phenomena which would free physics from its usual restriction to artificially simplified systems. The dream of every hydrodynamicist is an effective and complete theory of turbulence. Early workers on chaos thought they had found this philosopher's stone when they discovered that simple systems could have complex aperiodic behavior. They were disappointed when they discovered that chaos and turbulence were fundamentally different. But this early failure has not prevented significant advances in understanding a large class of previously inexplicable phenomena. Dynamical systems still seems the best approach to a theory of complexity.

References

[1] F. M. de Aguiar and S. M. Rezende, "Observation of subharmonic routes to chaos in parallel-pumped spin wave in yttrium iron garnet," *Phys. Rev. Lett.*, vol. 56, pp. 1070–1073, 1986.

[2] T. Allen, "On the arithmetic of phase locking: Coupled neurons as a lattice on R^2," *Physica*, vol. 6D, pp. 305–320, 1983.

[3] P. Alstrøm, B. Christiansen, P. Hyldgaard, M. T. Levinsen, and R. Rasmussen, "Scaling relations at the critical line and the period-doubling route for the sine map and the driven damped pendulum," *Phys. Rev. A*, vol. 34, pp. 2220–2233, 1986.

[4] F. T. Arecchi, W. Gadomski, and R. Menucci, "Generation of chaotic dynamics by feedback on a laser," *Phys. Rev. A*, vol. 34 (RC), pp. 1617–1620, 1986.

[5] A. Arneodo, G. Grasseau and E. J. Kosterlich, "Fractal dimensions and $f(\alpha)$ spectrum of the Hénon attractor," preprint, 1987.

[6] A. Arneodo and M. Holschneider, "Crossover effect in the $f(\alpha)$ spectrum for quasiperiodic trajectories at the onset of chaos," *Phys. Rev. Lett.*, vol. 58, pp. 2007–2010, 1987.

[7] V. I. Arnol'd, *Mathematical Methods of Classical Mechanics*. Berlin, Germany: Springer, 1974.

[8] D. G. Aronson, R. P. McGehee, I. G. Kevrekidis, and R. Aris, 'Entrainment regions for periodically forced oscillators," *Phys. Rev. A*, vol. 33 (RC), pp. 2190–2192, 1986.

[9] D. Auerbach, P. Cvitanovic, J. P. Eckmann, G. H. Gunaratne and I. Procaccia, "Exploring chaotic motion through periodic orbits," *Phys. Rev. Lett.*, vol. 58, pp. 2387–2390, 1987.

[10] A. Babloyantz, "Evidence of chaotic dynamics of brain activity during the sleep cycle," in *Dimensions and Entropies in Chaotic Systems*, (G. Mayer-Kress, Ed.) Berlin, Germany: Springer, 1986, pp. 241–245.

[11] H. Bai-Lin, *Chaos*. Singapore: World Scientific, 1984. (A collection of important papers with a useful introduction.)

[12] P. Bak, "The devil's staircase," *Physics Today*, vol. 39, pp. 38–45, Dec. 1986.

[13] J. Bélair and L. Glass, "Universality and self-similarity in the bifurcations of circle maps," *Physica*, vol. 16D, pp. 143–154, 1985.

[14] P. Bergé and M. Dubois, "Rayleigh–Bénard convection," *Contemp. Phys.*, vol. 25, pp. 535–582, 1984.

[15] P. Bergé, Y. Pomeau, and C. Vidal, *L'Ordre dans le Chaos: Vers une approche déterministe de la turbulence*. Paris, France: Hermann, 1984.

[16] D. J. Biswas and R. G. Harrison, "Experimental evidence of three-mode quasiperiodicity and chaos in a single longitudinal, multi-transverse-mode cw CO_2 laser," *Phys. Rev. A*, vol. 32, pp. 3835–3837, 1985.

[17] T. Bohr, P. Bak and M. H. Jensen, "Transition to chaos by interaction of resonances in dissipative systems. II. Josephson junctions, charge-density waves, and standard maps," *Phys. Rev. A*, vol. 30, pp. 1970–1981, 1984.

[18] T. Bohr and G. Gunaratne, "Scaling for supercritical circle-maps: Numerical investigation of the onset of bistability and period doubling," *Phys. Lett.*, vol. 113A, pp. 55–60, 1985.

[19] H. R. Brand, S. Kai, and S. Wakabayashi, "External noise can suppress the onset of spatial turbulence, preprint.

[20] A. Brandstäter, H. L. Swinney, and G. T. Chapman, "Characterizing turbulent channel flow," in *Dimensions and Entropies in Chaotic systems*, (G. Mayer-Kress, Ed.), Berlin, Germany: Springer, pp. 150–157, 1986.

[21] T. Braun, J. A. Lisboa, R. E. Francke, and J. A. C. Gallas,

"Observation of deterministic chaos in electrical discharges in gases," *Phys. Rev. Lett.*, vol. 59, pp. 613–616, 1987.
[22] S. E. Brown, G. Mozurkewich, G. Grüner, "Subharmonic Shapiro steps and devil's staircase behavior in driven charge-density-wave systems," *Phys. Rev. Lett.*, vol. 52, pp. 2277–2280, 1984.
[23] P. Bryant and C. Jeffries, "The dynamics of phase locking and points of resonance in a forced magnetic oscillator," preprint, 1986.
[24] ____, "Bifurcations of a forced magnetic oscillator near points of resonance," *Phys. Rev. Lett.*, vol. 53, pp. 250–253, 1987.
[25] R. V. Buskirk and C. Jeffries, "Observation of chaotic dynamics of coupled nonlinear oscillators," *Phys. Rev. A*, vol. 31, pp. 3332–3357, 1985.
[26] S. Chandrasekhar, *Hydrodynamic and Hydromagnetic Stability*. New York: Dover, 1981.
[27] K. Coffman, W. D. McCormick, and H. L. Swinney, "Multiplicity in a chemical reaction with one-dimensional dynamics" *Phys. Rev. Lett.*, vol. 56, pp. 999–1002, 1986.
[28] P. Collet and J.-P. Eckmann, *Iterated Maps on the Interval as Dynamical Systems*. Boston, MA: Birkhäuser, 1980.
[29] J. P. Crutchfield and B. A. Huberman, "Fluctuations and the onset of chaos," *Phys. Lett.*, vol. 77A, pp. 407–410, 1980.
[30] J. P. Crutchfield and N. H. Packard, "Symbolic dynamics of noisy chaos," *Physica*, vol. 7D, pp. 201–223, 1983.
[31] A. Cumming and P. S. Linsay, "Deviations from universality in the transition from quasi-periodicity to chaos," *Phys. Rev. Lett.*, vol. 59, pp. 1633–1636, 1987.
[32] P. Cvitanović, B. Shraiman, and B. Söderberg, "Scaling laws for mode lockings in circle maps," *Phy. Scr.*, vol. 32, pp. 263–270, 1985.
[33] P. Cvitanović, *Universality in Chaos*. Bristol, England: Adam Hilger, 1984. (A collection of reprints of important articles on birfurcation theory and chaos.)
[34] D. D'Humieres, M. R. Beasley, B. A. Huberman, and A. Libchaber, "Chaotic states and routes to chaos in the forced pendulum," *Phys. Rev. A*, vol. 26, pp. 3483–3496, 1982.
[35] R. E. Ecke and I. G. Kevrekidis, "Interactions of resonances and global bifurcations in Rayleigh–Bénard convection," preprint, 1987.
[36] J.-P. Eckmann and D. Ruelle, "Ergodic theory of chaos and strange attractors," *Rev. Mod. Phys.*, vol. 57, pp. 617–656, 1985.
[37] J.-P. Eckmann, "Roads to turbulence in dissipative dynamical systems," *Rev. Mod. Phys.*, vol. 53, pp. 643–654, 1981.
[38] I. R. Epstein, "Oscillations and chaos in chemical systems," *Physica*, vol. 7D, pp. 47–56, 1983.
[39] J. D. Farmer and J. J. Sidorowich, "Predicting chaotic time series," *Phys. Rev. Lett.*, vol. 59, pp. 845–848, 1987.
[40] ____, "Exploiting chaos to predict the future and reduce noise," preprint, 1988.
[41] A. P. Fein, M. S. Heutmaker, and J. P. Gollub, "Scaling at the transition from quasiperiodicity to chaos in a hydrodynamic system," *Phys. Scr.*, vol. T9, pp. 79–84, 1985.
[42] M. J. Feigenbaum, M. H. Jensen, and I. Procaccia, "Time ordering and the thermodynamics of strange sets," *Phys. Rev. Lett.*, vol. 57, pp. 1503–1506, 1987.
[43] M. J. Feigenbaum, "Universal behavior in nonlinear systems," *Physica*, vol. 7D, pp. 16–39, 1983.
[44] G. Gibson and C. Jeffries, "Observation of period doubling and chaos in spin-wave instabilities in yttrium iron garnet," *Phys. Rev. A*, vol. 29, pp. 811–818, 1984.
[45] L. Glass, M. R. Guevara, A. Shrier, and R. Perez, "Bifurcation and chaos in a periodically stimulated cardiac oscillator," *Physica*, vol. 7D, pp. 89–101, 1983.
[46] J. A. Glazier, M. H. Jensen, A. Libchaber, and J. Stavans, "The structure of Arnold tongues and the $f(\alpha)$ spectrum for period-doubling: Experimental results," *Phys. Rev. A*, vol. 34, pp. 1621–1624, 1986.
[47] J. A. Glazier, G. Gunaratne, and A. Libchaber, "$f(\alpha)$ curves—Experimental results," *Phys. Rev. A*, vol. 37, pp. 523–530, 1988.
[48] J. A. Glazier, G. Gunaratne, A. Libchaber, and M. Vinson, "Tongue crossing intermittency in Rayleigh–Bénard convection," preprint, 1988.
[49] J. P. Gollub and S. V. Benson, "Many routes to turbulent convection," *J. F. Mech.*, vol. 100, pp. 449–470, 1980.
[50] J. P. Gollub and A. R. McCarriar, "Convection patterns in Fourier space," *Phys. Rev. A*, vol. 26, pp. 3470–3476, 1982.
[51] J. P. Gollub, E. J. Romer, and J. E. Socolar, "Trajectory divergence for coupled relaxation oscillators: Measurements and models," *J. Stat. Phys.*, vol. 23, pp. 321–333, 1980.
[52] J. P. Gollub and H. L. Swinney, "Onset of turbulence in a rotating fluid," *Phys. Rev. Lett.*, vol. 35, pp. 927–930, 1975.
[53] P. Grassberger and I. Procaccia, "Characterization of strange attractors," *Phys. Rev. Lett.*, vol. 50, pp. 346–349, 1983.
[54] ____, "Estimation of the Kolomogorov entropy from a chaotic signal," *Phys. Rev. A*, vol. 28 (RC), pp. 2591–2593, 1983.
[55] C. Grebogi, E. Ott, and J. A. Yorke, "Are three-frequency quasiperiodic orbits to be expected in typical nonlinear systems?," *Phys. Rev. Lett.*, vol. 51, pp. 339–342, 1983.
[56] H. S. Greenside, A. Wolf, J. Swift, and T. Pignataro, "Impracticality of a box-counting algorithm for calculating the dimensionality of strange attractors," *Phys. Rev. A*, vol. 25, pp. 3453–3456, 1982.
[57] G. Grüner and A. Zettl, "Charge density wave conduction: A novel collective transport phenomenon in solids," preprint, 1987.
[58] M. R. Guevara, L. Glass, and A. Shrier, "Phase locking, period-doubling bifurcations, and irregular dynamics in periodically stimulated cardiac cells," *Science*, vol. 214, pp. 1350–1353, 1981.
[59] G. Gunaratne, M. H. Jensen, and I. Procaccia, "Universal strange attractors on wrinkled tori," *Nonlinearity*, vol. 1, pp. 157–180, 1988.
[60] E. G. Gwinn and R. M. Westervelt, "Intermittent chaos and low-frequency noise in the driven damped pendulum," *Phys. Rev. Lett.*, vol. 54, pp. 1613–1616, 1985.
[61] ____, "Frequency locking, quasiperiodicity, and chaos in extrinsic Ge," *Phys. Rev. Lett.*, vol. 57, pp. 1060–1063, 1986.
[62] ____, "Scaling structure of attractors at the transition from quasi-periodicity to chaos in electronic transport in Ge," *Phys. Rev. Lett.*, vol. 59, pp. 157–160, 1987.
[63] T. Halsey, M. H. Jensen, L. P. Kadanoff, I. Procaccia, and B. I. Shraiman, "Fractal measures and their singularities: The characterization of strange sets," *Phys. Rev. A*, vol. 33, pp. 1141–1151, 1986.
[64] H. Haucke, "Time-dependent convection in a ^{3}He–^{4}He Solution," Univ. California, San Diego, unpublished thesis.
[65] H. Haucke, R. E. Ecke, Y. Maeno, and J. C. Wheatley, "Noise-induced intermittency in a convecting dilute solution of ^{3}He in Superfluid ^{4}He," *Phys. Rev. Lett.*, vol. 53, pp. 2090–2093, 1984.
[64] H. Haucke and R. E. Ecke, "Mode locking and chaos in Rayleigh–Bénard convection," *Physica*, vol. 25D, pp. 307–329, 1987.
[67] H. Haucke and Y. Maeno, "Phase space analysis of convection in a ^{3}He-superfluid ^{4}He solution," *Physica*, vol. 7D, pp. 69–72, 1983.
[68] H. Haucke, Y. Maeno, and J. C. Wheatley, "Dimension and entropy for quasiperiodic and chaotic convection," in *Dimensions and Entropies in Chaotic Systems*, (G. Mayer-Kress, Ed.), Berlin, Germany: Springer, pp. 198–206, 1986.
[69] G. A. Held, C. Jeffries, and E. E. Haller, "Observation of chaotic behavior in an electron-hole plasma in Ge," *Phys. Rev. Lett.*, vol. 52, pp. 1037–1040, 1984.
[70] G. A. Held and C. Jeffries, "Spatial and temporal structure of chaotic instabilities in an electron-hole plasma in Ge," *Phys. Rev. Lett.*, vol. 55, pp. 887–890, 1985.
[71] ____, "Characterization of chaotic instabilities in an electron-hole plasma in germanium," in *Dimensions and Entropies in Chaotic Systems*, (G. Mayer-Kress, Ed.), Berlin, Germany: Springer, pp. 158–170, 1986.
[72] ____, "Quasiperiodic transition to chaos of instabilities in an electron-hole plasma excited by ac perturbations at one and two frequencies," *Phys. Rev. Lett.*, vol. 56, pp. 1183–1186, 1986.
[73] H. G. E. Hentschel and I. Procaccia, "The infinite number of generalized dimensions of fractals and strange attractors," *Physica*, vol. 8D, pp. 435–444, 1983.
[74] C. Huyghens, letter to his father, dated 26 Feb. 1665, *Ouevres completes de Christian Huyghens*, (M. Nijhoff, Ed.), The Hague, The Netherlands: Societé Hollandaise des Sciences, 1893, vol. 5, pp. 243–244. Cited in [12].
[75] H. Ikezi, J. S. deGrassie, and T. H. Jensen, "Observation of multiple-valued attractors and crises in a driven nonlinear circuit," *Phys. Rev. A*, vol. 28 (RC), pp. 1207–1209, 1983.
[76] M. H. Jensen, P. Bak, T. Bohr, "Transition to chaos by interaction of resonances in dissipative systems. I. Circle maps," *Phys. Rev. A*, vol. 30, pp. 1960–1969, 1984.
[77] M. H. Jensen, L. P. Kadanoff, A. Libchaber, I. Procaccia and J. Stavans, "Global universality at the onset of chaos: Results of a forced Rayleigh–Bénard experiment," *Phys. Rev. Lett.*, vol. 55, pp. 2798–2801, 1985.
[78] R. Keolian, L. A. Turkevich, S. J. Putterman, I. Rudnick, and J. A. Rudnick, "Subharmonic sequences in the Faraday experiment: Departures from period doubling," *Phys. Rev. Lett.*, vol. 47, pp. 1133–1136, 1981.
[79] S. Kim and S. Ostlund, "Simultaneous rational approximations in the study of hydrodynamic systems," *Phys. Rev. A*, vol. 34, pp. 3426–3434, 1986.
[80] ____, "Renormalization mappings of the two-torus," *Phys. Rev. Lett.*, vol. 55, pp. 1165–1168, 1985.
[81] E. J. Kosterlich and J. A. Yorke, "Noise reduction in dynamical systems," preprint, 1988.
[82] W. Lauterborn and E. Cramer, "Subharmonic route to chaos observed in acoustics," *Phys. Rev. Lett.*, vol. 47, pp. 1445–1448, 1981.
[83] A. Libchaber, "The onset of weak turbulence. An experimental introduction," in *Turbulence and Predictability in Geophysical Fluid Dynamics*, proc. Enrico Fermi Summer School, Corso LXXXVIII, Bologna, Italy: Societa Italiana di Fisica, pp. 17–28, 1985.
[84] A. Libchaber, S. Fauve, and C. Laroche, "Two-parameter study of the routes to chaos," *Physica*, vol. 7D, pp. 73–84, 1983.
[85] A. Libchaber and J. Maurer, "Une experience de Rayleigh–Bénard

de geometrie reduite; multiplication, accorchage et demultiplication de frequencies," *J. Phys. (Paris)*, vol. 41 C3, pp. C3-51–C3-56, 1980.
[86] P. S. Linsay, "Period doubling and chaotic behavior in a driven anharmonic oscillator," *Phys. Rev. Lett.*, vol. 47, pp. 1349–1352, 1981.
[87] E. Lorenz, "Deterministic nonperiodic flow," *J. Atmos Sci.*, vol. 20, pp. 130–144, 1963.
[88] *Low-Dimensional Conductors and Superconductors*, (D. Jérome and L. G. Caron, Eds.), London, England: Plenum, 1987, (contains an excellent sample of current work on charge density waves).
[89] R. S. Mackay and C. Tresser, "Transition to chaos for two-frequency systems," *J. Phys. Lett. (Paris)*, vol. 45, pp. L-741–L-746, 1984.
[90] ____, "Transition to topological chaos for circle maps," *Physica*, vol. 19D, pp. 206–237, 1986.
[91] ____, "Boundary of chaos for bimodal maps on the interval," and "Some flesh on the skeleton: The bifurcation structure of bimodal maps," (preprints).
[92] B. B. Mandelbrot, *Fractals, Form, Chance, and Dimension*, San Francisco, CA: Freeman, 1977. To be used only with caution.
[93] S. Martin and W. Martienssen, "Transition from quasiperiodicity into chaos in the periodically driven conductivity of BSN crystals," in *Dimensions and Entropies in Chaotic Systems*, (G. Mayer-Kress, Ed.), Berlin, Germany: Springer, pp. 191–197, 1986.
[94] S. Martin and W. Martienssen, "Circle maps and mode locking in the driven electrical conductivity of barium sodium niobate crystals," *Phys. Rev. Lett.*, vol. 56, pp. 1522–1525, 1986.
[95] J. Maurer and A. Libchaber, "Rayleigh–Bénard experiment in liquid helium; frequency locking and the onset of turbulence," *J. Phys. Lett. (Paris)*, vol. 40, pp. L-419–L-423, 1979.
[96] ____, "Effects of Prandtl number on the onset of turbulence in liquid ^{4}He," *J. Phys. Lett. (Paris)*, vol. 41, pp. L-515–L-518, 1980.
[97] R. M. May, "Simple mathematical models with very complicated dynamics," *Nature*, vol. 261, pp. 459–467, 1976.
[98] S. L. McCall, "Instability and regenerative pulsation phenomena in Fabry–Perot nonlinear optical media devices," *Appl. Phys. Lett.*, vol. 32, pp. 284–286, 1977.
[99] N. Metropolis, M. L. Stein, and P. R. Stein, "On finite limit sets for transformations of the unit interval," *J. Comb. Theor.*, vol. 15, pp. 25–44, 1973.
[100] T. Midavaine, D. Dangoisse, and P. Glorieux, "Observation of chaos in a frequency-modulated CO_2 laser," *Phys. Rev. Lett.*, vol. 55, pp. 1989–1992, 1985.
[101] F. C. Moon, J. Cusumano, and P. J. Holmes, "Evidence for homoclinic orbits as a precursor to chaos in a magnetic pendulum," *Physica*, vol. 24D, pp. 383–390, 1987.
[102] *Nonlinear Oscillations in Biology and Chemistry*, (S. Levin, Ed.), Berlin, Germany: Springer, 1986.
[103] S. Newhouse, D. Ruelle, and F. Takens, "Occurrence of strange axiom A attractors near quasi periodic flows on T^m, $m \geqslant 3$," *Comm. Math. Phys.*, vol. 64, pp. 35–40, 1978.
[104] P. C. Newell, "Attractor and adhesion in the slime mold dictyostelium," in *Fungal Differentiation*, (J. Smith, Ed.), New York: Marcel-Dekker, pp. 43–59, 1983.
[105] M. Octavio and C. R. Nasser, "Chaos in a dc-bias Josephson junction in the presence of microwave radiation," *Phys. Rev. B*, vol. 30 (RC), pp. 1586–1588, 1984.
[106] S. Ostlund, D. Rand, J. Sethna, and E. Siggia, "Universal properties of the transition from quasi-periodicity to chaos in dissipative systems," *Physica*, vol. 8D, pp. 303–342, 1983.
[107] R. Perez and L. Glass, "Bistability, period doubling bifurcations and chaos in a periodically forced oscillator," *Phys. Lett.*, vol. 90A, pp. 441–443, 1982.
[108] *Physica Scripta*, vol. T9, 1985, (contains a useful collection of experimental and theoretical papers on quasiperiodicity).
[109] R. W. Rollins and E. R. Hunt, "Exact solvable model of a physical system exhibiting universal chaotic behavior," *Phys. Rev. Lett.*, vol. 49, pp. 1295–1298, 1982.
[110] F. J. Romeiras, A. Bondeson, E. Ott, T. M. Antonsen, Jr., and C. Grebogi, "Quasiperiodically forced dynamical systems with strange nonchaotic attractors," *Physica*, vol. 26D, pp. 277–294, 1987.
[111] J.-C. Roux, R. H. Simoyi, and H. L. Swinney, "Observation of a strange attractor," *Physica*, vol. 8D, pp. 257–266, 1983.
[112] D. Ruelle and F. Takens, "On the nature of turbulence," *Comm. Math. Phys.*, vol. 20, pp. 167–192, 1971.
[113] F. S. Rys and A. Waldvogel, "Fractal shape of hail clouds," *Phys. Rev. Lett.*, vol. 56, pp. 784–787, 1986.
[114] M. Schell, S. Fraser, and R. Kapral, "Subharmonic bifurcation in the sine map: An infinite hierarchy of cusp bistabilities," *Phys. Rev. A*, vol. 28, pp. 373–378, 1983.
[115] J. P. Sethna, E. D. Siggia, "Universal transition in a dynamical system forced at two incommensurate frequencies," *Physica*, vol. 11D, pp. 193–211, 1984.
[116] R. S. Shaw, *The Dripping Faucet*. Santa Cruz, CA: Ariel, 1984.
[117] M. Sherwin, R. Hall, and A. Zettl, "Chaotic ac conductivity in the charge-density-wave state of $(TaSe_4)_2I$," *Phys. Rev. Lett.*, vol. 53, pp. 1387–1390, 1984.
[118] S. J. Shenker, "Scaling behavior in a map of a circle onto itself: Empirical results," *Physica*, vol. 5D, pp. 405–411, 1982.
[119] B. Shraiman, C. E. Wayne, P. C. Martin, "Scaling theory for noisy period-doubling transitions to chaos," *Phys. Rev. Lett.*, vol. 46, pp. 935–939, 1981.
[120] R. H. Simoyi, A. Wolf, and H. L. Swinney, "One-dimensional dynamics in a multicomponent chemical reaction," *Phys. Rev. Lett.*, vol. 49, pp. 245–248, 1982.
[121] C. W. Smith and M. J. Tejwani, "Bifurcation and the universal sequence for first-sound subharmonic generation in superfluid helium-4," *Physica*, vol. 7D, pp. 85–88, 1983.
[122] K. R. Sreenivasan, "Chaos in open flow systems," in *Dimensions and Entropies in Chaotic Systems*, (G. Mayer-Kress, Ed.), Berlin, Germany: Springer, pp. 222–230, 1986.
[123] J. Stavans, F. Heslot, and A. Libchaber, "Fixed winding number and the quasiperiodic route to chaos in a convective fluid," *Phys. Rev. Lett.*, vol. 55, pp. 596–599, 1985.
[124] J. Stavans, S. Thomae, and A. Libchaber, "Experimental study of the attractor of a driven Rayleigh–Bénard system," in *Dimensions and Entropies in Chaotic Systems*, (G. Mayer-Kress, Ed.), Berlin, Germany, Springer, pp. 207–214, 1986.
[125] J. Stavans, "Experimental study of quasiperiodicity in a hydrodynamical system," *Phys. Rev. A*, vol. 35, pp. 4314–4328, 1987.
[126] R. L. Stratonovich, *Topics in the Theory of Random Noise* [2 vols.], trans. R. A. Silverman, New York: Gordon and Breach, 1967.
[127] Z. Su, R. W. Rollins, and E. R. Hunt, "Measurements of $f(\alpha)$ spectra of attractors at transitions to chaos in driven resonator systems," *Phys. Rev. A*, vol. 36, pp. 3515–3517, 1987.
[128] H. L. Swinney, "Observations of order and chaos in nonlinear systems," *Physica*, vol. 7D, pp. 3–15, 1983.
[129] H. L. Swinney and J. Maselko, "Comment on 'Renormalization, unstable manifolds, and the fractal structure of mode locking'," *Phys. Rev. Lett.*, vol. 55, p. 2366, 1985.
[130] P. Szépfalusy and T. Tél, "Dynamical fractal properties of one-dimensional maps," *Phys. Rev. A*, vol. 35 (RC), pp. 47–480, 1987.
[131] F. Takens, "Detecting strange attractors in turbulence," in *Dynamical Systems and Turbulence*, (D. A. Rand and L.-S. Young, Eds.) Berlin, Germany: Springer, 1981.
[132] T. Tél, "Dynamical spectrum and thermodynamic functions of strange sets from an eigenvalue problem," preprint.
[133] J. Testa, J. Pérez, and C. Jeffries, "Evidence for universal behavior in a driven nonlinear oscillator," *Phys. Rev. Lett.*, vol. 48, pp. 714–717, 1982.
[134] C. Tresser, private communication.
[135] J. S. Turner, J.-C. Roux, W. D. McCormick, and H. L. Swinney, "Alternating periodic and chaotic regimes in a chemical reaction —Experiment and theory," *Phys. Lett.*, vol. 85A, pp. 9–12, 1981.
[136] A. T. Winfree, *The Geometry of Biological Time*. Berlin, Germany: Springer, 1980.
[137] ____, *When Time Breaks Down*, Princeton, NJ: Princeton Univ., 1987.
[138] H. G. Winful, Y. C. Chen, and J. M. Liu, "Frequency locking, quasiperiodicity, and chaos in modulated self-pulsing semiconductor lasers," *Appl. Phys. Lett.*, vol. 48, pp. 616–618, 1986.

✠

James A. Glazier was born in Cambridge, MA, in 1962. He received the B.A. degree in physics and mathematics from Harvard University, Cambridge, MA, in 1984 and the M.S. degree in physics from the University of Chicago, Chicago, IL, in 1987.

His interests are dynamical systems and disorder.

✠

Albert Libchaber was born in Paris, France, in 1934. He received the Ph.D. degree from the Ecole Normale Supèrieure in 1965.

He is presently professor of Physics at the University of Chicago. Previously he was directeur de recherche at the Ecole Normale Supèrieure, Paris. His interests are all aspects of non-linear physics. He was co-recipient in 1986 of the Wolff prize in Physics. In 1986 he received a MacArthur fellowship.

Dr. Libchaber is a member of the AAAS and the French Academie des Sciencès.